Southern African Field Archaeology
2025 Vol. 20: Article 3408
Research report (peer-reviewed): Received September 2024; Revised January 2025; Published July 2025
DOI: https://doi.org/10.36615/safa.20.3408.2025

ISSN 1019-5785
ISSN 2789-1844

Dune, outcrop, and pan sediments from the southern Kalahari Basin: A geoarchaeological case study from the Kgalagadi district, Botswana

Inèz Faul [a, *], Taylor Grandfield [b], Stefan Dreibrodt [c], Sarah Mothulatshipi [d], Phillip Segadika [e], Christopher Green [a], Marine Frouin [b] & Michaela Ecker [a]

[a]Institute of Pre- and Protohistoric Archaeology, Kiel University, Johanna-Mestorf-Str. 2-6, 24118, Kiel, Germany
[b]Department of Geosciences, Stony Brook University, 255 Earth and Space Sciences Building, Stony Brook, NY 11794-2100, USA
[c]State Office for Monument Preservation Baden-Württemberg, Fischersteig 9, 78343 Gaienhofen-Hemmenhofen, Germany
[d]Department of History, University of Botswana, Private Bag UB 0022, Gaborone, Botswana
[e]Department of National Museum and Monuments, Khama Crescent, Gaborone, 9999, Botswana
**Corresponding author email: ifaul@ufg.uni-kiel.de*

ABSTRACT
Research from the southern Kalahari Basin (previously considered to be of limited Pleistocene archaeological significance) has provided evidence of human occupation. Surveys and excavations conducted in the Kgalagadi District near Tsabong in south-western Botswana have revealed a plethora of archaeological evidence. The region includes geomorphological features, including dunes, low quartzite hills, and pans. Duricrust formations are visible inside the pans. Previous research suggests that the pans form in topographical low points and likely already existed during the Pleistocene, while lunette dunes accumulated from deflated pan sediment during recent drying periods. However, in this region, these features have not been analysed in a geoarchaeological context, which can provide insight into the formation of archaeological sites. We investigated the mechanisms involved in the deposition of pan, dune, and sandy outcrop sediment by applying a multi-method analysis to thirty sediment samples. Analysis of pan samples reveals the presence of mostly intergrade duricrusts, with some calcretes present. Pan sediment containing fragmented ostracod valves in juvenile instars indicates post-mortem transport (taphocoenosis), and along with the diatoms (*Campylodiscus* sp.), are indicative of a brackish to saline water body. Inner dune samples share more similarities with pan sediments than with the red sand samples, as they contain higher concentrations of calcium oxide and some contain calcite and sepiolite. Particle size distributions change from unimodal in the outcrops and red dunes, to polymodal in the pans, suggesting that runoff during the wet season contributes to site formation. Sediment deflation by wind contributed to artefacts being exposed on the surfaces of the outcrops. This study therefore identifies three main site formation processes, namely deflation, runoff, and various duricrust formations, which provides insights into the environmental and climatic conditions that influenced human habitation in the Kalahari.

Keywords: Kalahari, duricrusts, sedimentology, geoarchaeology

1. Introduction

Most evidence for human evolution and associated cognitive milestones during the Pleistocene in southern Africa comes from cave sites on the southern Cape Coast (such as Blombos Cave [Henshilwood et al. 2018], Pinnacle Point [Marean 2010], and Klasies River [Wurz 2008]), as well as a few inland cave sites like Wonderwerk Cave (Berna et al. 2012) and Border Cave (Sievers et al. 2022). The focus on cave sites often overlooks the potential contributions of open-air archaeological

sites to interpret the archaeological record. Notable open-air sites, such as Florisbad (Grün et al. 1996; Toffolo et al. 2017) in the Free State and Kathu Pan (Wilkins 2017; Lukich et al. 2020), Ga-Mohana (Wilkins 2023), and Canteen Kopje (e.g., Kuman et al. 2020) in the Northern Cape, have all assisted in verifying the archaeological importance of the interior. However, many of these sites are located on the southern boundary of the Kalahari in South Africa, with fewer archaeological sites reported in Botswana and other areas of the Kalahari landscape. Recent research in the Makgadikgadi Palaeolake in northern Botswana has inferred the use of the lakebed by early modern humans during dry periods after lake-level high stands in the late Pleistocene (Burrough et al. 2022; Staurset et al. 2023; Thomas et al. 2022). These and similar findings have challenged ideas from the previous century proposing that aridity hindered hominins from settling in the Kalahari (Helgren & Brooks 1983). Despite archaeological research in the Kalahari becoming more prevalent, there is still a lack of focus on the south-western part of the semi-desert in Botswana.

The town of Tsabong (26°1'12" S 22°24'20" E) is the administrative capital of the Kgalagadi district, located approximately 600 km south-west of Gaborone. Despite the area's uniform and flat landscape, distinctive morphological features are present, including pans (seasonal water bodies), lunette dunes (transverse dunes) on the southern leeward side of most pans, and low quartzite hills (for example, Maleshe Hill) (Fig. 1). These features can be used as proxies for establishing palaeoenvironmental and depositional contexts (Lancaster 1978; Watts 1980; Ringrose et al. 1999; Telfer & Thomas 2006; Telfer et al. 2009; Lukich 2019; Thomas et al. 2022). The archaeological potential of this region has largely been noted in unpublished field reports from Seo Pan by the late Terry Hardaker and Phillip Segadika. A study by Ecker et al. (2023) has confirmed the area is rich in quartzite stone tools belonging primarily to Earlier to Middle Stone Age (ESA and MSA) typologies. These surface scatter sites are often located on raw material outcrops near pans (Ecker et al. 2023). However, a comprehensive geoarchaeological analysis of the pans, outcrops, lunette dunes, and duricrust formations in south-western Botswana, where the lithics are located, has not yet been conducted.

This study employs a multi-method approach to fill this gap. It presents one of the first geoarchaeological studies using particle size analysis (Mastersizer Hydro 2000), loss-on-ignition (LOI), X-ray diffraction (XRD), Energy-Dispersive X-ray Fluorescence (ED-XRF), and the analysis of microfossils in this area. This analysis provides valuable information on the various site formation processes at archaeological sites in the Kgalagadi district. Here, we present the results from the analysis of 30 sediment samples excavated from archaeological sites near the villages of Maleshe and Maralaleng (Fig. 1). The sites near Maleshe village include Maleshe Quarry (MAL Quarry), Maleshe Lunette Dunes 1 (MLD 1) and 2 (MLD 2), Letlakhane Quarry (LET) and Itireleng (ITI). The quarry site samples are from exposed profiles previously used for gravel quarrying. The Maralaleng sites comprise of Maralaleng Quarry (MAR-QCE), Maralaleng Mud Pit (MAR-G1), and Test pits 1 (MAR-T1) and 2 (MAR-T2). Sample abbreviations and contexts are provided in Table 1. These results are compared to existing literature to gain insight into how these archaeological test pits, geotrenches, and exposed profiles relate to the pan and dune sediments in this region, along with insights into the formation of those sediments.

2. Background

The southern Kalahari Basin is host to the Kalahari Group sediments. The most notable of the Kalahari lithologies is the red, wind-blown sand, known as the Kalahari Sands. The Kalahari Sands are characterised as fine to medium sand with sub-rounded to rounded particles (Thomas & Shaw 1991). The visible bedrocks in the study area are quartzites from the Olifantshoek Sequence (Tidi 1994). This area is situated in the Savanna biome of southern Africa (Rutherford et al. 2006). The southern Kalahari Basin experiences highly variable annual mean precipitation (approximately 150-300 mm) (Thomas & Shaw 1991; Byakatonda et al. 2018; Thomas & Wiggs 2022) and is covered by bush and shrub savannah vegetation (Lancaster 1978; Werger 1978), thus classifying it as a semi-desert. Despite this classification, research suggests that the Kalahari was more inhabitable during parts of the Pleistocene, experiencing considerable wet phases (Helgren & Brooks 1983; Wilkins et al. 2021; Lukich & Ecker 2022). The Kalahari drains internally and retains little surface water, even

during the rainy season (October-April) (Thomas & Shaw 1991). Moisture fluctuations and deficits (due to high evaporation ratios) contribute to the formation of duricrusts, such as calcretes (Watts 1980; Alonso-Zarza & Wright 2010), over extended periods.

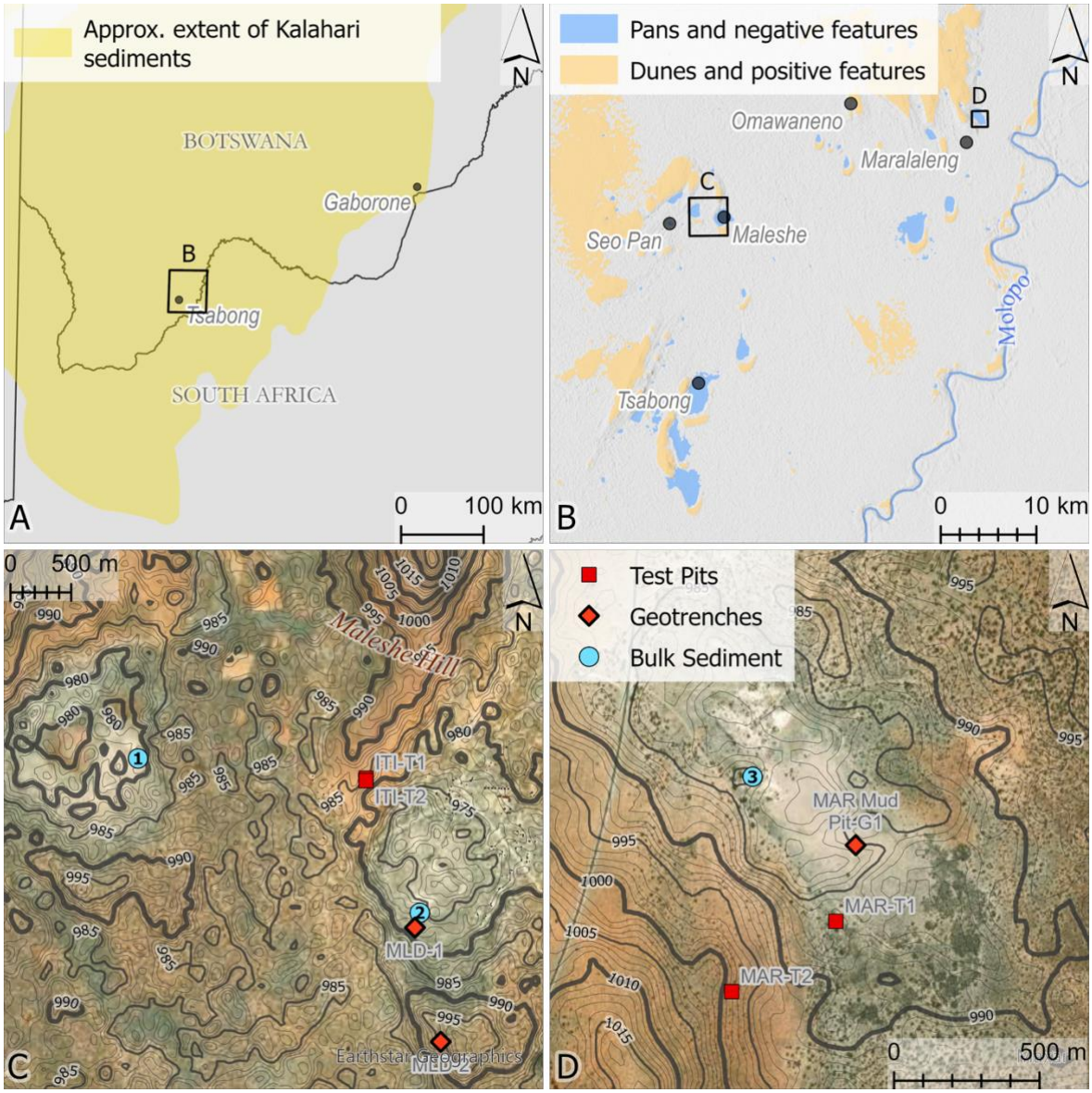

Figure 1. The study area. a) The extent of the Kalahari sediments (after Thomas 1988) in Botswana and South Africa and the geographical location of the town of Tsabong; inset square highlights the study area. b) Map of the Tsabong region; dunes and other elevated (positive) features, and negative features (pans and depressions) are indicated, with the inset squares showing the two areas compared in this study. c) The bulk sediment sampling locations in the Maleshe area within archaeological test pits (ITI-T1 and ITI-T2), depicted as red squares, and exposed profiles (1. LET 2. MAL Quarry) shown as blue dots; geotrenches MLD 1 and MLD 2 are depicted as red diamonds. d) The sampling locations in the Maralaleng area are denoted with red squares depicting archaeological test pits MAR-T1 and MAR-T2 and the exposed profile (3. MAR-QCE) as a blue circle; geotrench MAR-G1 is indicated by a red diamond.

Pans occur in topographical low points (Shaw & Thomas 1997; Schüller et al. 2022). Pans in the southern Kalahari Basin are broadly described as having saline to clayey surfaces (Schüller et al. 2022). Research conducted at Witpan in South Africa (southern Kalahari) suggests that the pans consist of mostly silt and clay, with some aeolian, sand-sized quartz grains that likely settled on the pan floor during a wetter-than-present phase (Telfer et al. 2009). The pans are often accompanied by two lunette dunes (crescent-shaped transverse dunes [Hills 1940]); an outer, larger 'red' dune and a

smaller dune with pale-coloured sediment that represent primarily Holocene accumulations caused by sediment deflation, especially from the last 2000 years, according to OSL dating (Telfer & Thomas 2006; Schüller et al. 2022). The lunette dunes are usually located on the south-western side of the pans. The formation of the fringing lunette dunes is argued to be the result of periods of aridity that cause sediment to deflate from the dry pan surface (Lancaster 1978; Thomas & Wiggs 2022; Schüller et al. 2022), but can also occur as a result of sediment moving towards the downward margin by wave action during wet periods (Bowler 1986; Thomas & Wiggs 2022).

Table 1. Table showing the names and abbreviations of test pits, as well as the type of pit.

Name of exposure	Study samples	Type of exposure and context
Iterileng Test Pit 1 (ITI-T1)	ITI-T1	Archaeological test pit on outcrop with Kalahari sand cover.
Maleshe Quarry (MAL Quarry)	MAL Quarry Bed 1 (surface); MAL Quarry Bed 2; MAL Quarry Bed 3; MAL Quarry Bed 4 (Upper); MAL Quarry Bed 4 (Middle); MAL Quarry Bed 4 (Lower); MAL Quarry Bed 5	Exposed profile in quarry.
Maleshe Lunette Dune 1 (MLD 1)	MLD 1.1; MLD 1.2; MLD 1.3; MLD 1.4	Geotrench on inner dune section.
Maleshe Lunette Dune 2 (MLD 2)	MLD 2.1; MLD 2.2; MLD 2.3	Geotrench on outer dune section.
Letlhakane Profile 1 (LET Profile 1)	LET Quarry Profile 1 Bed 1; LET Quarry Profile 1 Bed 2; LET Quarry Profile 1 Bed 3	Geotrench in quarry to extend an already exposed profile.
Letlhakane Profile 2 (LET Profile 2)	LET Quarry Profile 2	Geotrench in quarry to extend an already exposed profile.
Maralaleng Quarry Calcrete Exposure 1 (MAR-QCE1)	MAR QCE 1 Surface; MAR QCE 1 Bed 1; MAR QCE 1 Bed 2	Exposed profile in quarry.
Maralaleng Test Pit 1 (MAR-T1)	MAR-T1 Bed 1 Upper; MAR-T1 Bed 1 Lower; MAR-T1 Bed 2 (Calcrete)	Archaeological test pit on inner dune section.
Maralaleng Test Pit 2 (MAR-T2)	MAR-T2	Archaeological test pit on outcrop with Kalahari sand cover.
Maralaleng Mud Pit Goetrench 1 (MAR-G1)	MAR-G1 Bed 1; MAR-G1 Bed 2 (Upper); MAR-G1 Bed 2 (Lower); MAR-G1 Bed 3	Geotrench inside the pan at MAR.

Duricrust formation is a dominant feature in the Kgalagadi landscape, especially on the pan surfaces, and is characteristic of arid and semi-arid regions (Netterberg 1980; Watts 1980; Warren 1983; Nash et al. 2004). Duricrusts are near-surface crusts that have been chemically precipitated and are classified based on the dominant mineral of cementation (e.g., Nash & Shaw 1998; Kampunzu et al. 2007; Nash 2022). Various types of duricrusts have been identified throughout the Kalahari, such as calcrete (Netterberg 1969; Goudie 1972; Watts 1980; Nash & McLaren 2003), silcrete (Summerfield 1983a; Nash & Shaw 1998; Webb & Nash 2020; Nash et al. 2022), and ferricrete (Munyikwa et al. 2000). The most predominant types of duricrust identified in the southern Kalahari Basin in Botswana are calcretes, silcretes, and intergrade duricrusts (Nash & Shaw 1998; Nash et al. 2004; Nash 2022). Calcretes are cemented by calcium carbonate ($CaCO_3$), whereas silcrete is cemented by silica (SiO_2). Silcrete-calcrete, or cal-silcrete intergrade duricrusts, refers to a duricrust cemented by a mixture of silica and calcium carbonate. Calcrete, silcrete, and intergrade duricrusts are all secondary formations that have precipitated over a host sediment.

Calcretes are terrestrial accumulations of $CaCO_3$ found in semi-arid environments where formation is influenced by factors such as rapid evaporation, groundwater fluctuations, and $CaCO_3$ availability (Netterberg 1969; Watts 1980; Alonso-Zarza & Wright 2010). Watts (1980) conducted a mineralogical analysis on pans north of Gaborone in Botswana and suggested that the clay minerals palygorskite and sepiolite can be linked to the formation of calcrete in this area, but that sepiolite is more common in mature calcrete formations. The calcretes described by Watts (1980) likely developed during periods of increased aridity and are composed of high magnesium calcite. Groundwater calcretes (non-pedogenic) have been described in dry river valleys in central Botswana by Nash and McLaren (2003). These calcretes are described as being more than 4 m-thick, structureless, cemented, and becoming less indurated with depth (Nash & McLaren 2003). Numerous phases of cementation were identified in single profiles, relating to both capillary rise and formation

in the vadose zone (Nash & McLaren 2003). Remains of molluscs (*Melanoides tuberculate*) and diatoms (*Campylodiscus* sp.) were found, suggesting an environment with fresh to brackish water conditions when the valleys were active (Nash & McLaren 2003).

A duricrust is considered a silcrete when it has >85% weight SiO_2 (Summerfield 1983b; Nash et al. 1994; Nash 2022). Case studies from the Kalahari Desert in Botswana suggest that silcretes in this region have formed in arid and alkaline environments (Nash et al. 1994). When conducting bulk sediment geochemistry, it is important to note that silcrete geochemistry is affected by the host sediment over which the silcrete formed (Nash et al. 1994). Intergrade duricrusts are widespread in the Kalahari and have been recorded in Namibia and Botswana (Nash & Shaw 1998). The presence of silcrete, calcrete, and intergrade duricrusts indicate the water's pH, as calcretes are more likely to develop at a high pH and silcretes at a lower pH (compared to calcretes) (Nash & Shaw 1998).

3. Site descriptions

Archaeological sites within the villages of Maleshe and Maralaleng were recorded during the 2022 field season. Geoarchaeological samples were collected from three locations in Maleshe (MAL Quarry, ITI, and LET) and from four areas around Maralaleng Pan (MAR-QCE 1; MAR-G1; MAR-T1; MAR-T2) in the village of Maralaleng.

Maleshe

MAL Quarry is a pan with an area of 2.45 km^2 according to the Shuttle Radar Topography Mission (SRTM) elevation model. Observed duricrust profiles within the pan suggest various stages of development. Maleshe Pan is associated with MLD 1 and MLD 2, which are situated southwest of Maleshe village, and artefacts pertaining to the Iron Age have been described on the outer dune (Ecker et al. 2023).

ITI is an open-air site located at the base of Maleshe Hill. The vegetation in the area consists mostly of thorny bushes, some thorny trees, and a few patches of grass. Artefacts relating to ESA and MSA typologies have been previously documented (Ecker et al. 2023). ITI-T1 (Fig. 2) is an archaeological test pit on a quartzite outcrop covered by red sand. ITI-T2 (see supporting online material [SOM] 1 Fig. 1 and Table 1) is a test pit adjacent to ITI-T1. Additional information about all samples is provided in SOM 1 (Table 1) and SOM 2 (Table 1).

LET is a pan site situated between Seo Pan and ITI (Ecker et al. 2023) that has an area of 1.37 km^2 according to the SRTM model. Duricrust profiles are exposed at the surface due to modern quarrying. The profiles at LET, visibly angled on a slope, are located close to an outcrop where lithics have been found (Ecker et al. 2023). LET Pan has an accompanying lunette dune on the southern leeward side, but the lunette dune was not sampled for this study.

Figure 2. Profile image from archaeological test-pit ITI-T1 (northern profile) located on a quartzite outcrop covered in Kalahari Sand.

Maralaleng
Maralaleng Pan has an area of 1.55 km^2 and it is more vegetated than the other pans mentioned in this study. Various small exposed duricrust profiles are visible near the lowest point of the pan. Maralaleng Pan does not have prominent lunette dunes like the other pans described above, however, an elevated area caused by a quartzite outcrop on the south-western side of the pan is visible (Fig. 1d). MAR-T1 is associated with the white inner dune and MAR-T2 is associated with the outcrop.

4. Materials and methods

Fieldwork method and strategy
Profiles exposed from gravel extraction for road construction were identified at Maleshe Quarry and Maralaleng Pan. These profiles were photographed, drawn, and documented, with samples collected from each identifiable layer. At the dunes and outcrops, archaeological test pits and geotrenches were excavated using trowels and spades. The archaeological test pits, each measuring 1 m^2, were excavated by hand in 10 cm spits using trowels, while geotrenches were dug with a spade without the use of spits. Table 1 lists which sites were exposed profiles, geotrenches, and archaeological test pits. In general, the upper 10 cm of each profile was excluded from sampling to avoid disturbed surface sediment.

Sediment samples were collected in the field during July/August 2022. Each sample was taken from a clearly visible stratigraphic layer, or at regular intervals when stratigraphy was not visible. SOM 1 Table 1 summarises the geoarchaeological field observations made in 2022, detailing the depth of each bulk sediment sample, the profile from which it was excavated, and the GRADISTAT (Blott & Pye 2001) sorting and textural groups.

Study sites
At the Maleshe Pan, the test pits ITI-T1 and ITI-T2 contained a high number of large angular gravels and exhibited no clear stratigraphy (also see SOM 1, Fig. 1, Table 1). Very fine plant roots were visible throughout the profiles. There was little to no void space, with the profiles being clast-supported, where the red sand matrix filled the spaces between clasts. ESA and MSA artefacts made from quartzite have been reported from these test pits (Ecker et al. 2023; Winterhalder 2023).

Two geotrenches (MLD 1 & MLD2) and one exposed profile (MAL Quarry) associated with Maleshe Pan were analysed. Bioturbation, in the form of ant holes, termite holes, and plant material, was present across the profiles studied from Maleshe Pan. The two geotrenches were opened on the inner and outer dunes, respectively. The inner dune (MLD 1) has yellow-white sediment and no visible stratigraphy (Fig. 3). Gastropod shells were excavated from MLD 1 and four bulk sediment samples were taken. The outer red dune (MLD 2; Fig. 4) is the larger lunette dune on the southern side of MAL Quarry (the pan site) and had surface scatters of late ESA, MSA, Later Stone Age (LSA), and Iron Age artefacts. The geotrench was dug downslope and southwest of the village of Maleshe. Although the MLD 2 profile lacked clear stratigraphy, darker patches of sediment were visible, and the presence of roots was visible within the profile. A total of three bulk sediment samples were taken from here. MAL Quarry (Fig. 5) is an exposed profile inside Maleshe Pan where seven bulk sediment samples were collected. At LET two exposed profiles were recorded. Both LET Profile 1 and LET Profile 2 are duricrust profiles (Figs 6 & 7). Three bulk sediment samples were collected from LET Profile 1 and one bulk sediment sample was collected from LET Profile 2.

At Maralaleng Pan, two test pits (MAR-T1 & MAR-T2), one geotrench (MAR-G1) and one exposed profile (MAR-QCE1) were recorded and sampled. Geotrench MAR-G1 is located towards the centre of the pan and reached a depth of 110 cm before a hard duricrust layer was reached (Fig. 8). A total of four bulk sediment samples were collected from this trench. Exposed quarrying profile MAR-QCE1 (Fig. 9) is located north-east of MAR-G1 and is in an area where duricrust extraction was visible. This exposed profile was 150 cm deep and three bulk sediment samples were taken. Archaeological test pit MAR-T1 (Fig. 10) is in the area between the pan and the outcrop and reached a depth of 150 cm. No clear stratigraphy was visible in MAR-T1, except for the transition of upper sandy deposits to lower

deposits that contained calcite nodules. Three bulk sediment samples were collected from MAR-T1 in addition to excavated snail shells and fragments of ostrich eggshell. MAR-T2 (Fig. 11) is located on the raw material outcrop where red dune sand is visible on the hill slope outcrop. MAR-T2 reached a depth of 37 cm, and one bulk sediment sample was collected. Although less artefacts were noted in comparison to the ITI test pits, ESA and MSA lithics were recorded during the 2022 survey on the surface of the southern slope and the pan floor (Ecker et al. 2023).

Figure 3. Photograph of geotrench MLD 1 located on the inner dune associated with Maleshe Pan. Bulk sediment sampling locations are marked with circles, while the triangles denote OSL sampling locations. Sample IDs correspond with bed names. Each pole section=25 cm.

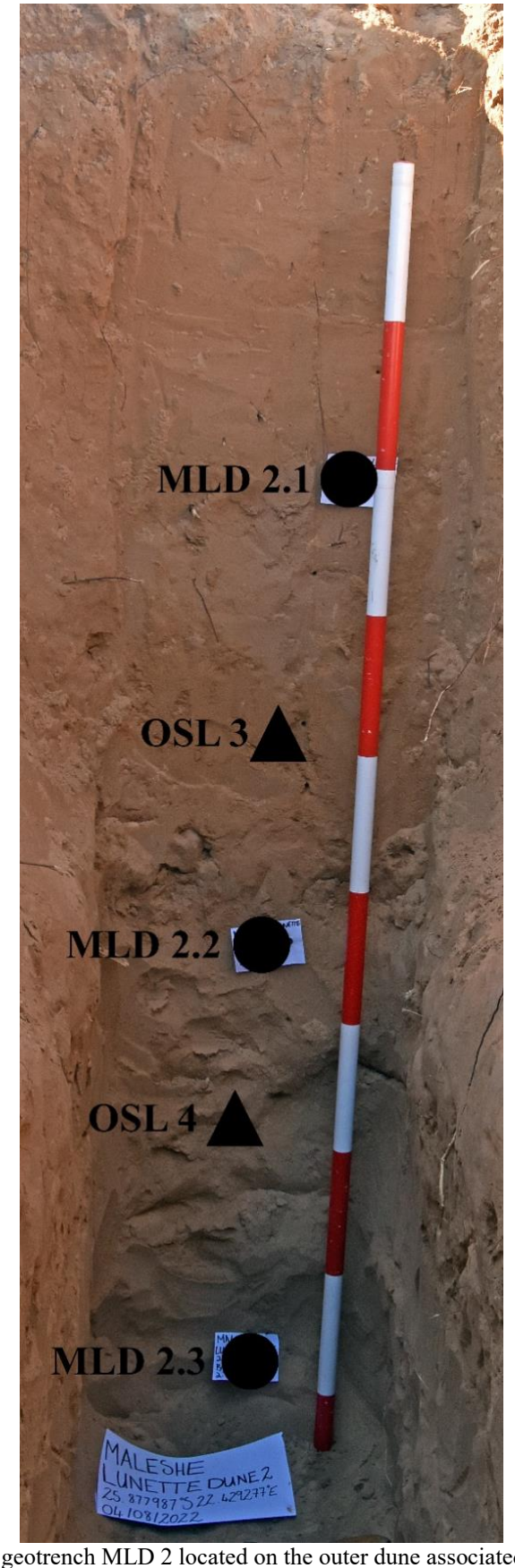

Figure 4. Photograph of geotrench MLD 2 located on the outer dune associated with Maleshe Pan. Bulk sediment sampling locations are marked with circles, while the triangles denote OSL sampling locations. Sample IDs correspond with bed names. Each pole section=25 cm.

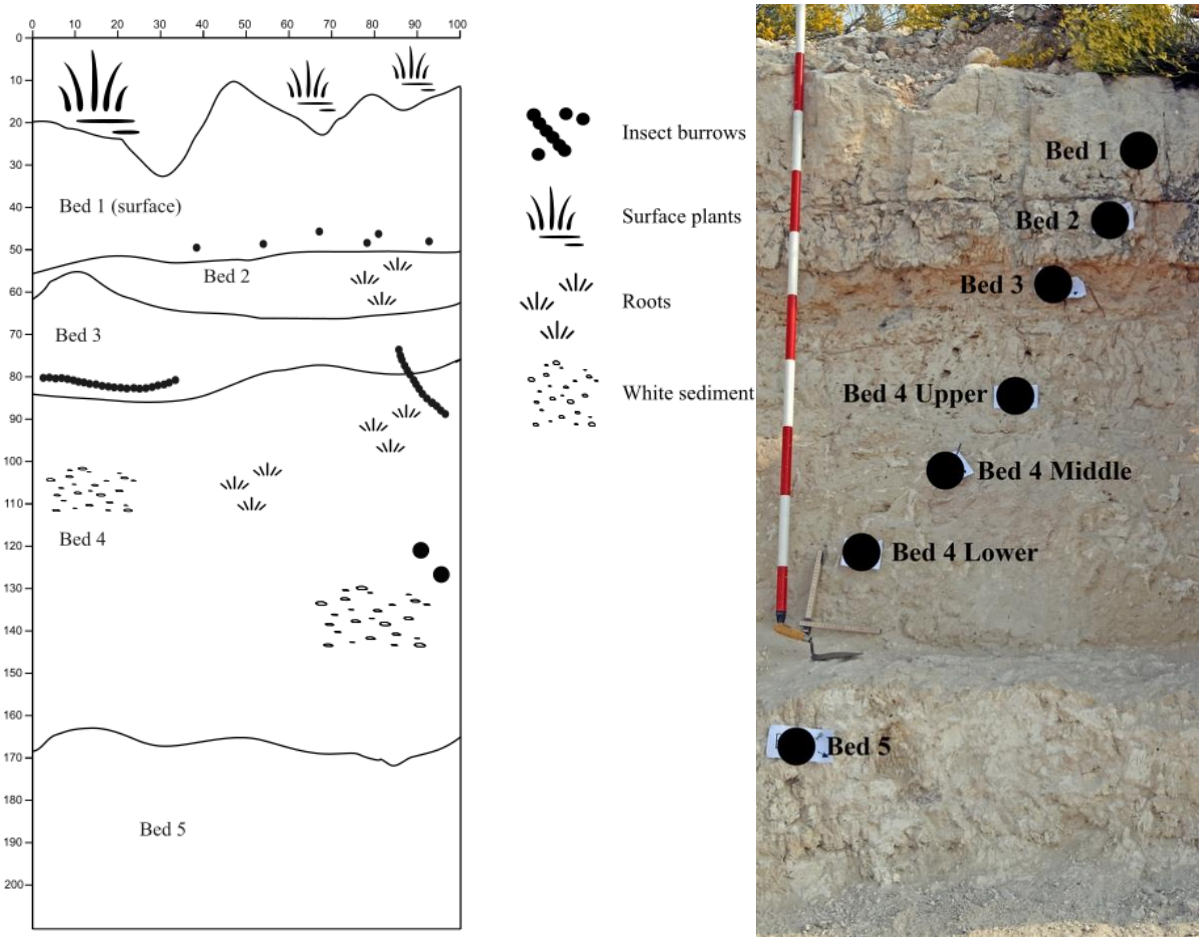

Figure 5. Profile drawing (left, with legend to the right of the drawing) and photograph (right) of exposed duricrust profile MAL Quarry, located inside Maleshe Pan. Black circles represent the locations where bulk sediment samples were collected. Sample IDs correspond with bed names. Each pole section=25 cm.

Analytical methods

Pan and dune geomorphology – GIS: Pan extents were calculated by performing a fill operation in GIS to fill in all self-contained negative features on the elevation model. This technique, typically used in hydrological modelling to ensure that water does not stop when there is no exit from a cell (Tarboton et al. 1991; Planchon & Darboux 2002), was adapted for this study. The original elevation model was subtracted from the filled surface, resulting in a model showing only the extent and depths of all self-contained negative features. A 2 m cut-off depth was then applied to separate these features into individual objects. In this landscape, most of the larger self-contained negative features are pans.

For the dunes, the same operation was applied to an inverted elevation model, resulting in self-contained positive features, which were also separated using the 2 m cut off. Most of these features are hills or ranges of hills, but dunes could be manually extracted based on their form and relative location to pans.

Pan and dune volumes were calculated by isolating a single feature, summing all depths/heights of the cells within the feature, and multiplying by the areal extent of each cell. This method, while an approximation, is relatively straightforward and should be reasonably accurate, as all calculations are derived from the same model and subject to the same constraints. Higher quality elevation models, such as those derived from LiDAR data, would produce more precise results, but such models are not currently available for this area.

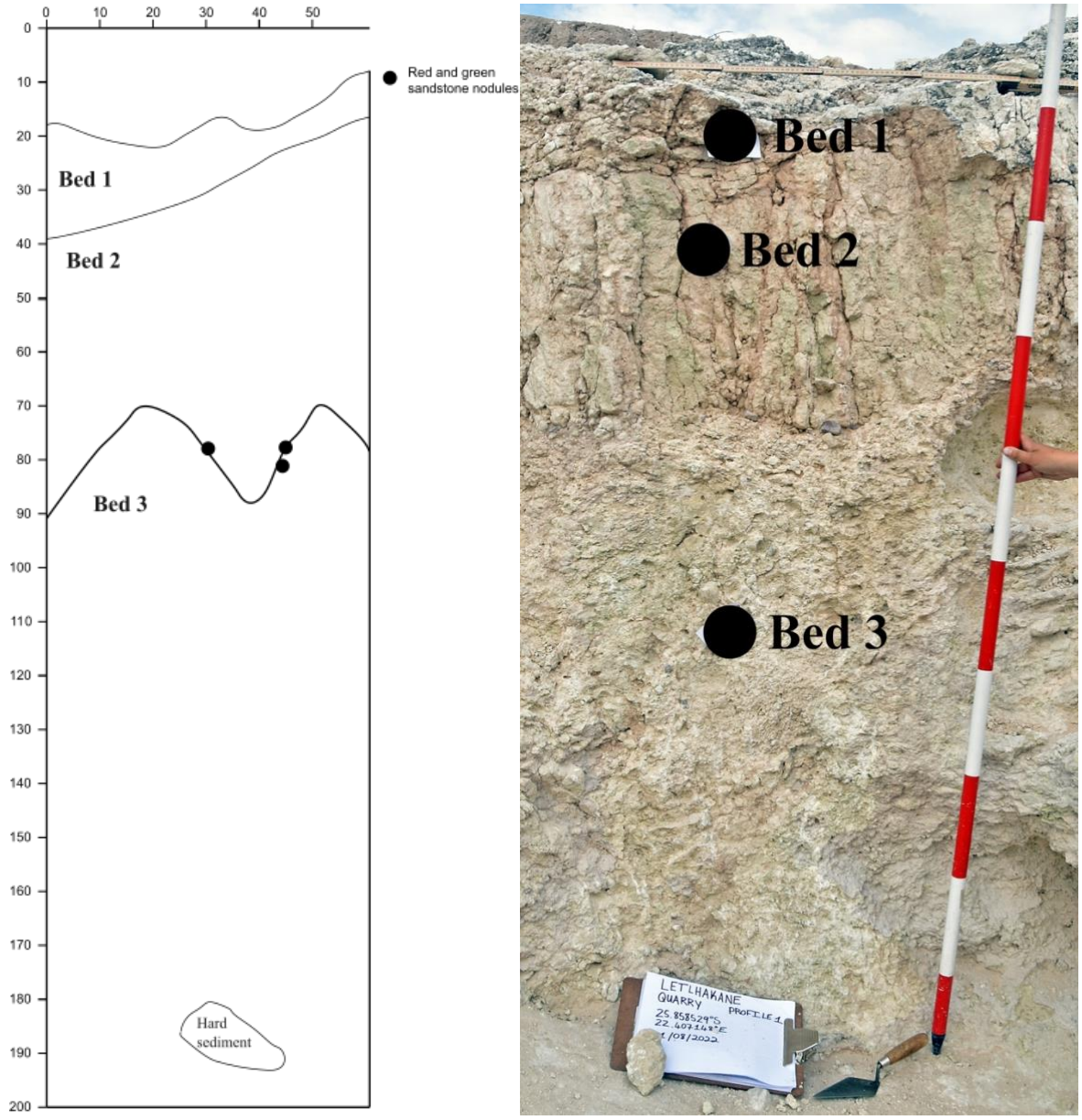

Figure 6. Profile drawing (left, with legend to the right of the drawing) and photograph (right) of the exposed LET Profile 1. Locations of bulk sediment samples are represented by black circles. Sample IDs correspond with bed names. Each pole section=25 cm.

Bulk sediments were collected from exposed profiles at each visible stratigraphic layer using either a trowel or hammer and chisel. Thirty sediment samples are discussed here. The bulk sediment was divided in half in the lab. One half was kept as an archive for microfossil analysis, while the other half was homogenised into fractions larger and smaller than 2 mm. The fraction <2 mm was then used for the LOI, Mastersizer 2000, ED-XRF, and XRD analyses.

LOI was applied using a protocol adapted from Heiri et al. (2001). Approximately 5 g of sediment was dried overnight (>12 hrs) at 105°C to remove any water content. Samples were then heated at 550°C in a muffle furnace for 2 hrs to estimate the relative organic matter. Finally, samples were burnt at 940°C for two hours to approximate inorganic carbonate content.

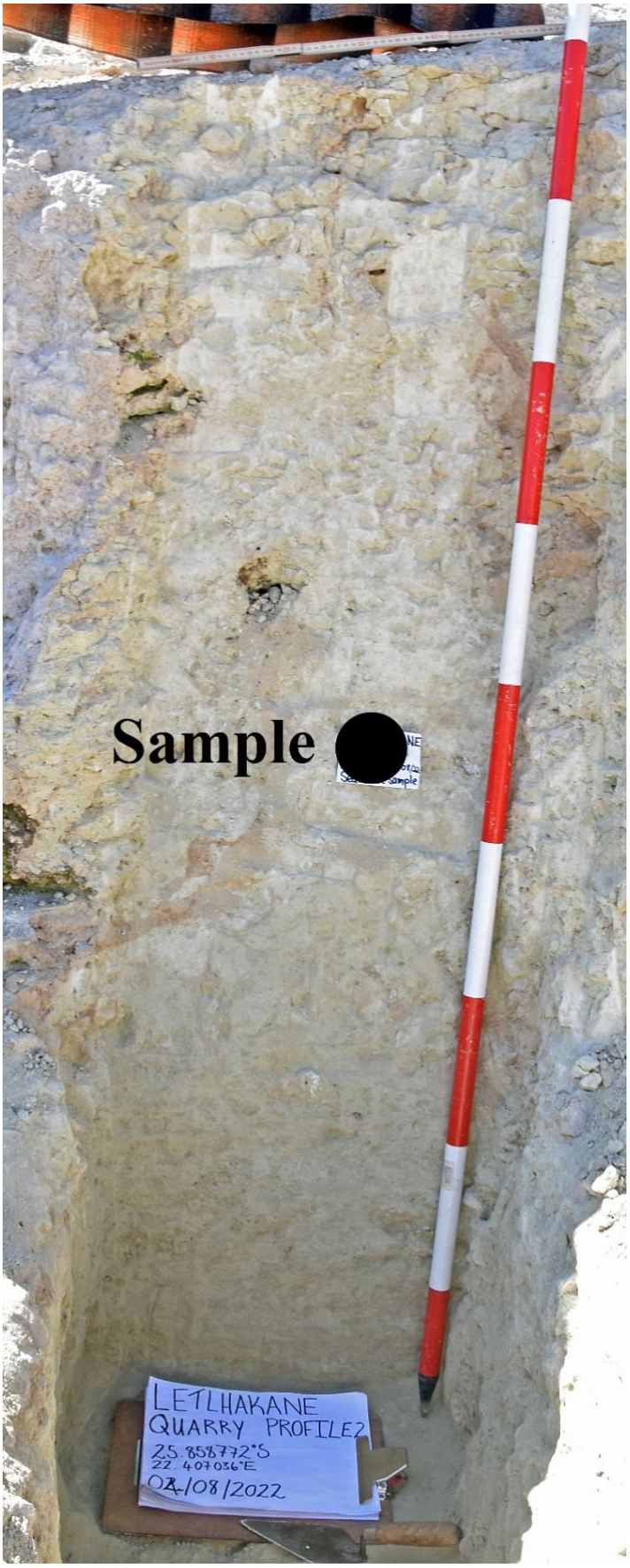

Figure 7. Photograph of exposed profile LET Profile 2 located inside LET Pan. The location of a bulk sediment sample is represented by the black circle. Sample ID is LET Profile 2. Each pole section=25 cm.

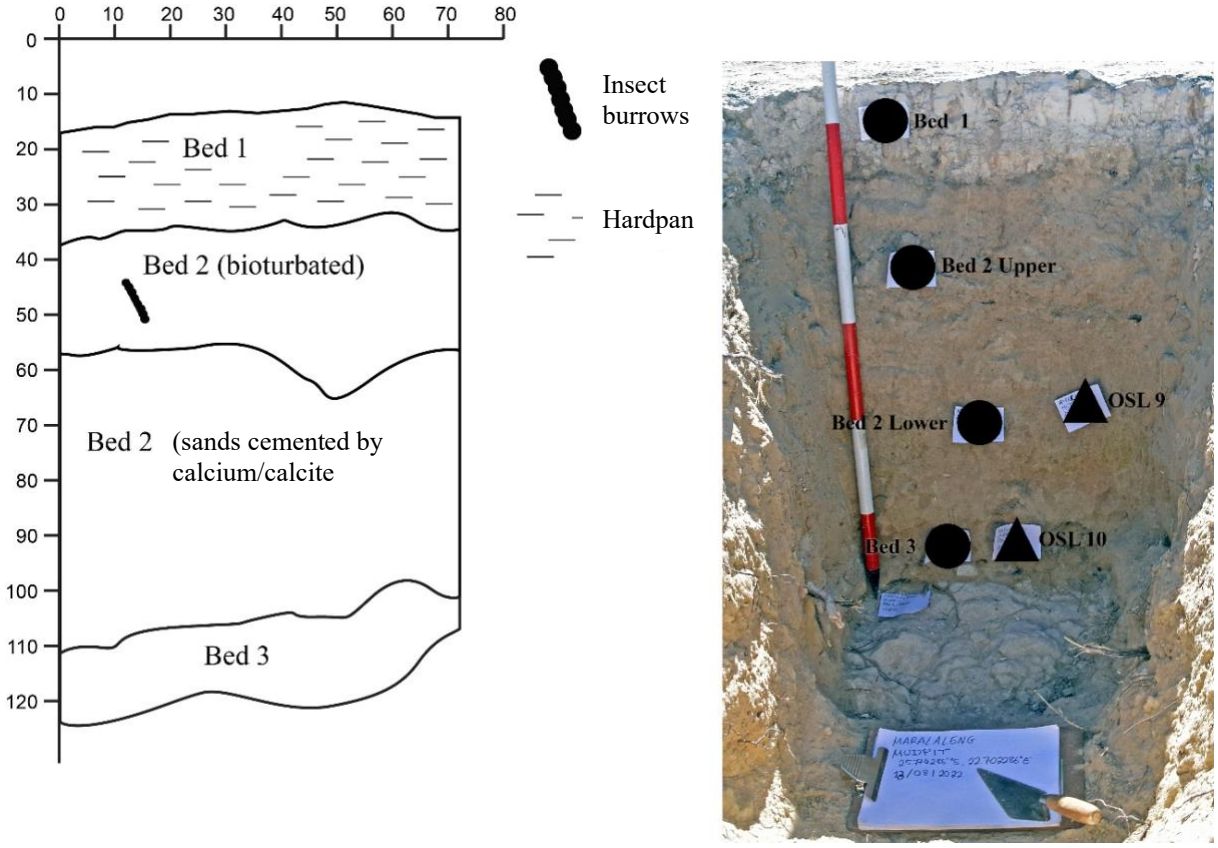

Figure 8. Profile drawing (left, with the legend to the right of the drawing) and photograph (right) of geotrench MAR-G1, located inside Maralaleng Pan. Bulk sediment sampling locations are illustrated with circles, while the triangles indicate OSL sampling locations. Sample IDs correspond with bed names. Each pole section=25 cm.

Between 1.0 and 1.6 g of sediment was used for the Mastersizer particle size analysis. A standard protocol from the Institute for Ecosystem Research (Kiel University) was followed. In this procedure, organic matter was removed by adding 35% hydrogen peroxide (H_2O_2) in 10 ml increments, along with 5-10 ml of distilled water. The samples were then placed in a thermal bath at 60°C until the reaction subsided. One to two additions of 35% H_2O_2 were necessary, as the samples did not contain much organic material. After removing organic matter, two to three rounds of Na-acetate-acetic acid (sodium acetate) buffer were added to the samples to remove the inorganic carbonates. The samples were then placed in a water bath at 60°C again. Following this, the supernatant was removed with a pipette, and 1-3 ml of 1 M magnesium chloride ($MgCl_2$) solution and 10 ml of distilled water was added to the samples. Magnesium chloride was used to speed up the sedimentation process. The supernatant was removed again, 0.5 ml of 0.1 M sodium pyrophosphate ($Na_4P_2O_7$) and 5-10 ml of distilled water was added. Finally, the samples were placed onto a shaker platform overnight. The Mastersizer 2000 (Hydro) was used to establish particle size distributions between 0.02-2000 µm using laser diffraction. GRADISTAT (Microsoft Excel) program version 9.1 (Blott & Pye 2001) was used to gather information on particle size statistics. The size classification of particle sizes was modified by Blott and Pye (2001), from Udden (1914) and Wentworth (1922), to categorise the sediment. The program uses Folk and Ward's (1957) descriptive terms.

To determine the elemental composition of the sediment, an Ametek Spectro Xepos Energy Dispersive XRF machine was used on the samples. Sub-samples of the <2 mm sediment fraction were dried in an oven at 40°C for a minimum of one week. The samples were then homogenised into a <60 µm fraction using an agate mill and covered with a 4 µm plastic film. Each sample was measured for a total of 600 seconds. In this context, when using the ED-XRF, CaO and SiO2 are the main elements

used to determine whether a sample is a calcrete, silcrete, or intergrade duricrust. The ED-XRF results assume that all CaO is related to CaCO3 and that all SiO2 is related to either silcrete formation or the original Kalahari host sediment. This approach is used in conjunction with XRD. For selected ground samples (n=9) previously analysed using ED-XRF, an XRD mineral analysis was performed using a D8 Discover by Bruker AXS (Cu K-α radiation with a wavelength of approximately 1.54 Å; step size: 0.037° 2 theta; count time: 2 s/step; measuring range: 2°-70° 2 theta). The XRD device uses theta-theta geometry and has a copper X-Ray source. The homogenised <60 µm fraction was also used for XRD. The samples were selected to further establish the presence of calcification (and CaCO3) and the presence of clay minerals in certain contexts. Minerals from the XRD analysis were identified using the High Score Plus software by PANalytical version 4.8 (4.8.0.255.18) (Degen et al. 2014).

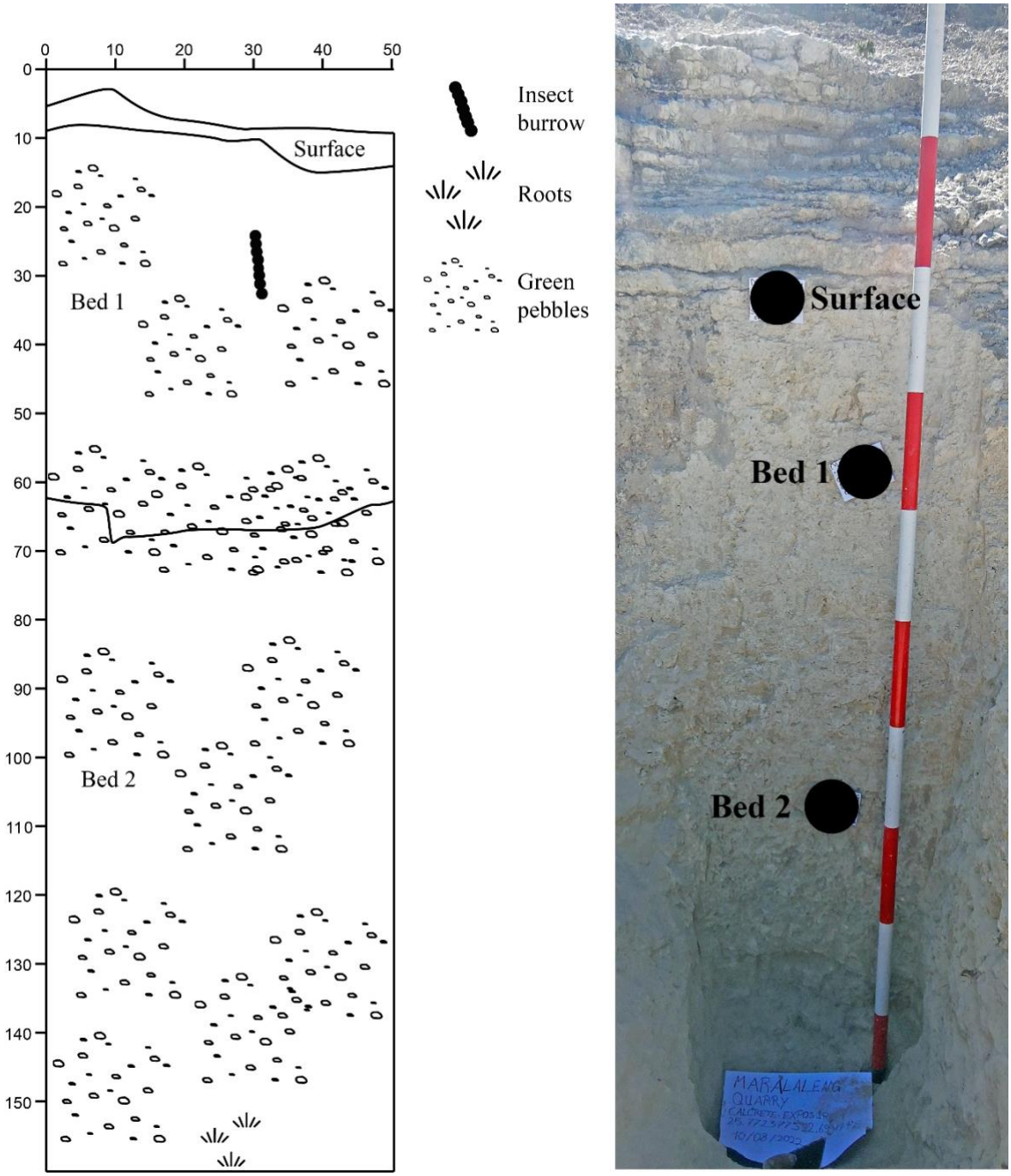

Figure 9. Profile drawing (left, with the legend to the right of the drawing) and photograph (right) of exposed duricrust profile MAR-QCE 1, located inside Maralaleng Pan. Bulk sediment sampling locations are marked with circles. Sample IDs correspond with bed names. Each pole section=25 cm.

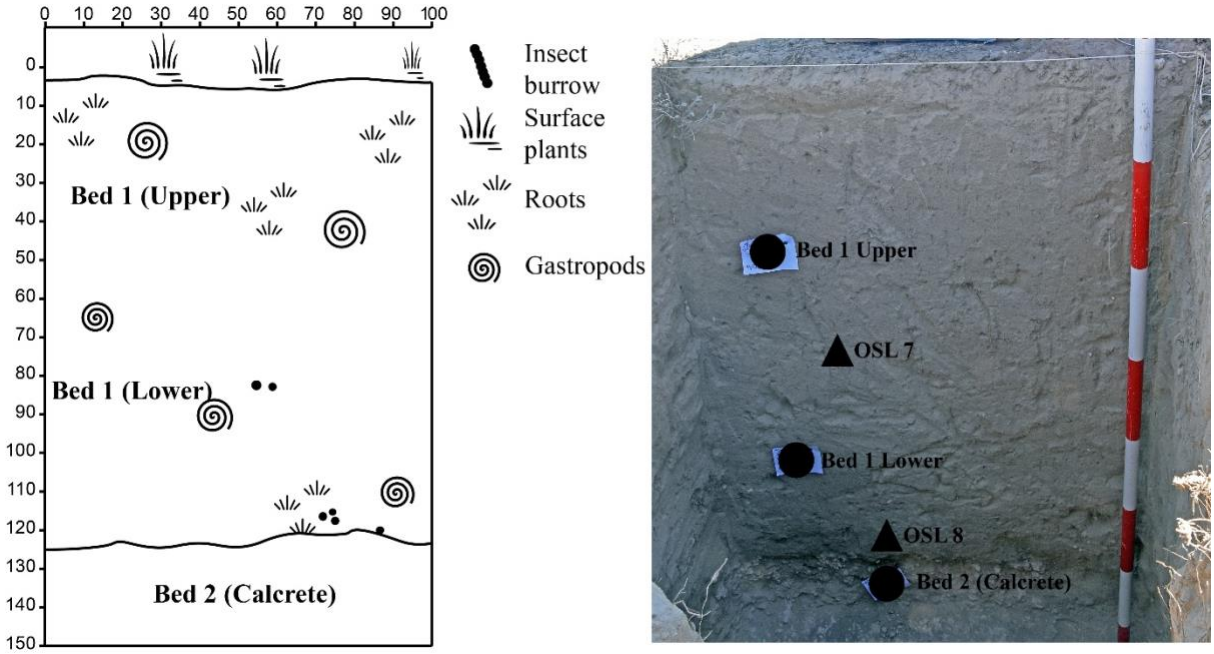

Figure 10. Profile drawing (left, with the legend to the right of the drawing) and photograph (right) of archaeological outcrop test-pit MAR-T1, located in Maralaleng Pan. Bulk sediment sampling locations are marked with circles along with OSL sampling locations (triangles). Sample IDs correspond with bed names. Each pole section=25 cm.

Figure 11. Profile image taken from archaeological test-pit MAR-T2 (southern profile) located on a quartzite outcrop covered in Kalahari Sand.

Sub-samples of approximately ≤50 g from each of the >2 mm un-homogenised bulk sediment samples were washed using deionised water through 63 µm, 125 µm, 250 µm, and 1 mm nest sieves (Horne & Siveter 2016). Samples with larger cemented clasts were first disaggregated in deionised water on a shaker platform overnight before wet sieving. Thereafter, the sieved samples were placed into an oven at 40-60°C until dry. Samples were then analysed on a black picking tray. A fine-picking brush was used to pick out specimens of interest and mounted on a micropalaeontological slide with water-soluble glue. A COXEM EM-30AXN was used to take SEM images of microfossils.

To determine which components are responsible for the main variables between all the samples analysed (Bialik et al. 2021), a Principal Component Analysis (PCA) was conducted using the Paleontological Statistics Software Package version 4.17 (PAST – PAleontological STatistics)

(Hammer & Harper 2001). Before the statistical analysis, all data (ED-XRF, LOI and particle size analysis) were normalised in MS Excel using the logarithmic function (Filzmoser et al. 2009).

5. Results

The outcrop samples, ITI-T1 and MAR-T2 and dune samples from MLD 2 contain very little organic matter and inorganic carbonates, especially compared to inner dune samples MLD 1 and MAR-T1 (Fig. 12). At MLD 1 there is an increase in carbonate content, but a decrease in organic matter with depth. The inorganic carbonate content decreases from MLD 2.1 to MLD 2.2 but increases again in MLD 2.3. The organic content remains fairly consistent, besides a slight decrease, from MLD 2.2 to MLD 2.3 (Fig. 12). The LOI results for MAR-T1 indicate that the inorganic carbonate content increases slightly with depth and is more abundant in the sample than in the organic matter throughout the sequence. At MAR-T2 the organic matter was more abundant in the inorganic carbonate (Fig. 12). The samples with the highest inorganic carbonates were all from the inner dunes, namely MAR-T1 and MLD 1. Red dune and outcrop samples contained more organic matter than inorganic carbonates.

Pan sediments generally had higher concentrations of inorganic carbonates (Fig 13). The inorganic carbonate content decreases with depth at MAL Quarry, but becomes more enriched in the lowermost bed, MAL Quarry Bed 5 (22.3%). Additionally, organic matter content also increases in MAL Quarry Bed 5 (Fig. 13). The percentage of inorganic carbonate content fluctuates at MAR-QCE 1, where Bed 1 has the highest abundance. MAR-QCE 1 Bed 2 has the lowest abundance of inorganic carbonates. The amount of inorganic carbonates decreases with depth at MAR-G1 (Fig. 13).

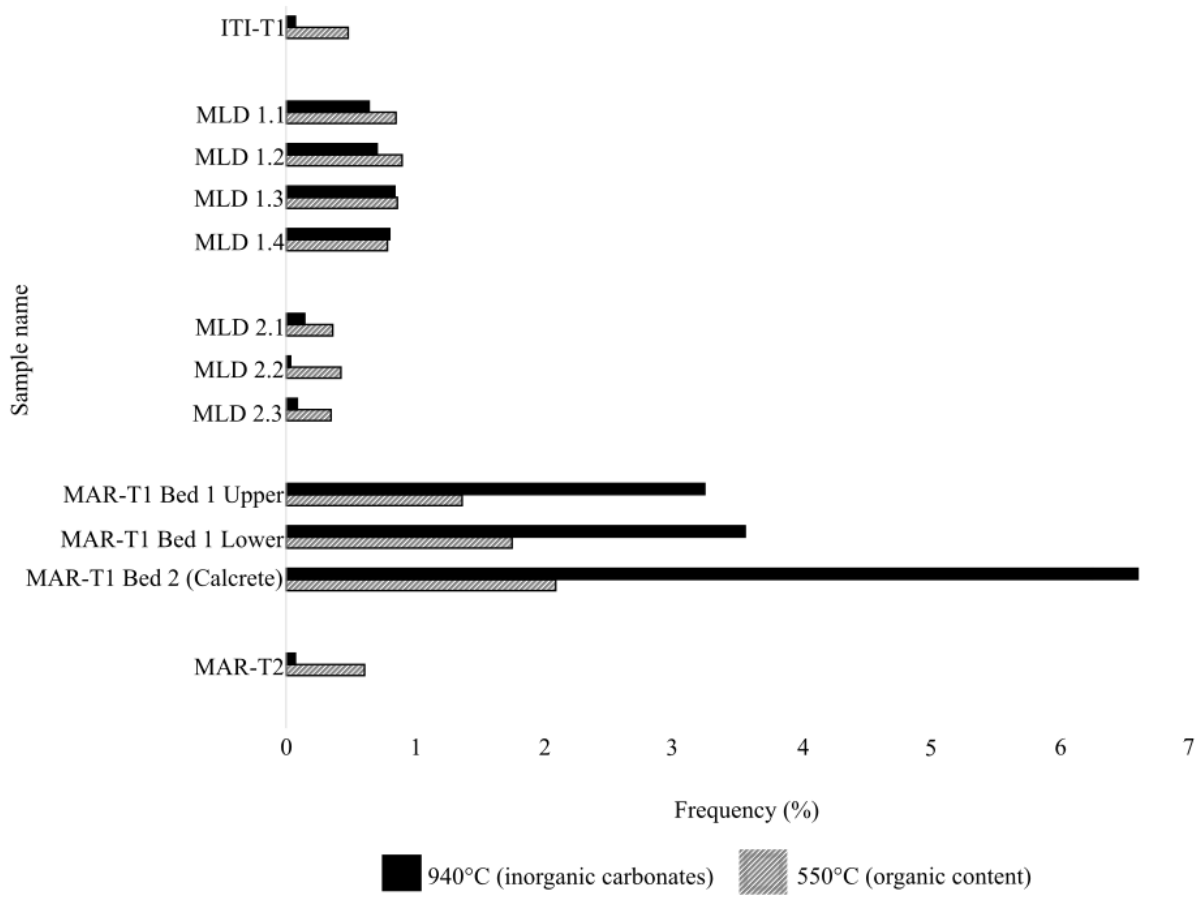

Figure 12. LOI results for organic matter (burnt at 550°C) and inorganic carbonate (burnt at 940 °C) for outcrop and dune samples.

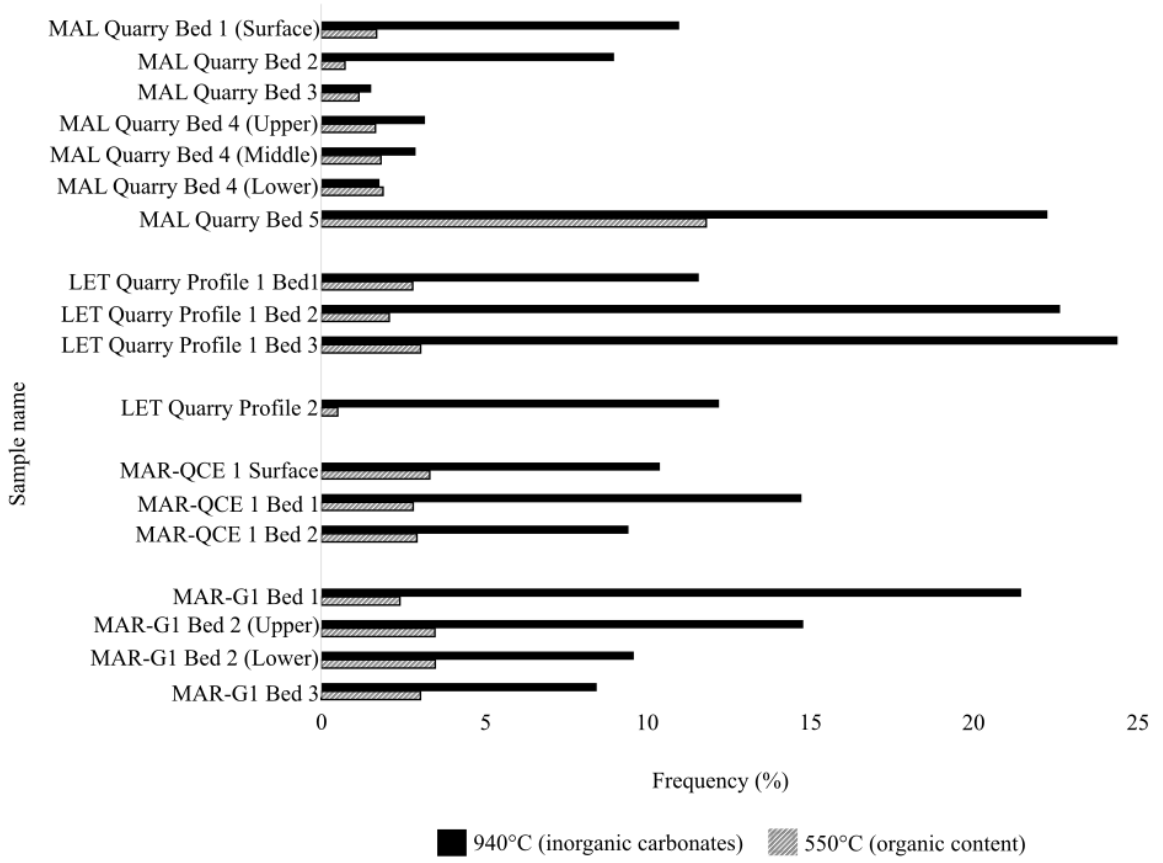

Figure 13. LOI results for organic matter (burnt at 550°C) and inorganic carbonate (burnt at 940 °C) for pan samples.

Particle size distributions from the Maleshe area and Maralaleng Pan ranged from well-sorted to very poorly sorted sediment, depending on the site and the geoproxy analysed (Fig. 14). In general, the red dune and outcrop sediments are well sorted, whereas pan and inner dune samples are more poorly sorted (Fig. 14). The particle size data are provided in SOM 2 Table 1.

The outcrop sample from ITI-T1 consist mostly of medium sand-sized sediment (250-500 μm), but include some silt-sized sediment as well (Fig. 14). ITI-T1 has a unimodal distribution and is moderately sorted. Similarly, MAR-T2 is moderately sorted with a unimodal distribution, having most particles in the medium sand category (250-500 μm). However, MAR-T2 contains 2.7% silt (when all silt classes are counted together) and 0.3% clay. The red outer dune samples from MLD 2 are mostly sand-sized with unimodal distributions that become finer with depth. The inner, white dune, MLD 1, has a unimodal distribution but is comprised of poorly sorted sand. Similarly to MLD 1, the upper two samples from inner dune MAR-T1 (MAR-T1 Upper; MAR-T1 Lower) have unimodal distributions but are also poorly sorted. The lowermost layer in the profile, MAR-T1 Bed 2, was noted as being an unconsolidated sand layer with calcite nodules. The MAR-T1 Bed 2 sediments have a bimodal distribution and are poorly sorted.

At MAL, Quarry Bed 1 (surface) and Quarry Bed 2 have poorly sorted unimodal distributions. Quarry Beds 3 and 4 (upper) are poorly sorted with bimodal distributions. MAL Quarry Bed 4 (middle) sediments are poorly sorted, but with a unimodal distribution. MAL Quarry Bed 4 (lower) exhibits a unimodal, poorly sorted distribution, with 86.6% sand, 13.4% silt and no clay component. MAL Quarry Bed 5 is very poorly sorted and unimodal, consisting of 56.8% sand, 41.7% silt, and 1.5% clay. Samples from LET Profile 1 and 2 are mostly in the medium to fine sand categories. The samples are all unimodal and very poorly sorted, except LET Profile 1 Bed 3, which has a bimodal distribution and is very poorly sorted.

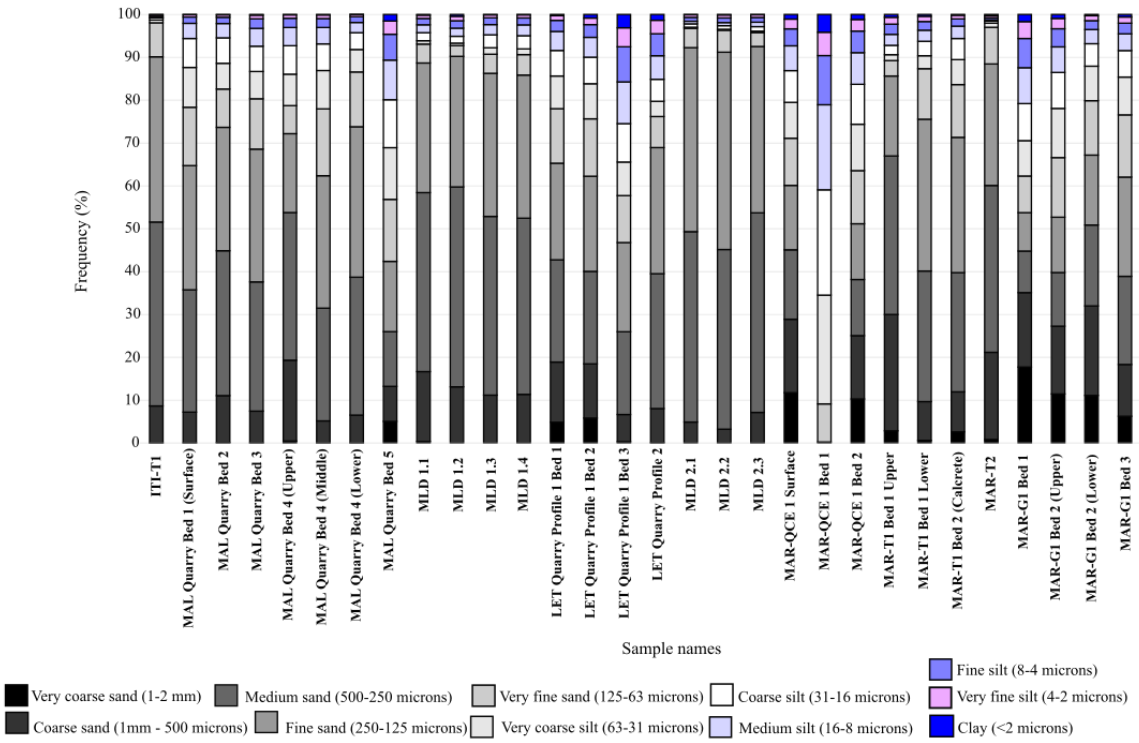

Figure 14. Particle size distribution percentages of all samples calculated using the GRADISTAT program in MS Excel by Blott and Pye (2001).

MAR-QCE 1 surface exhibits a unimodal distribution and is very poorly sorted, with 71.1% sand, 27.8% very coarse to very fine silt, and 1.1% clay. MAR-QCE 1 Bed 1 is also unimodal and poorly sorted. Unlike the previous samples, the main grain size distribution is in the very coarse to very fine silt category (86.7%), with 9.1% sand component, and 4.2% clay. MAR-QCE1 Bed 2 has a bimodal distribution that is very poorly sorted. Sand makes up most of the grain size distribution, whereas very coarse to very fine silt makes up 35.3% and clay makes up 1.2%. Geotrench MAR-G1 Bed 1 is a trimodal distribution that is very poorly sorted and consists of mostly very coarse to very fine sand (62.3%), very coarse silt to very fine silt (36%), and a minor component of clay (1.7%). MAR-G1 Bed 2 Upper has a bimodal distribution that is very poorly sorted. MAR-G1 Bed 2 Lower is a unimodal distribution and the sample is very poorly sorted. Here, the clay fraction only contributes to 0.3% of the total particle sizes, while very coarse to fine sand is at 79.9%. MAR-G1 Bed 3 has a unimodal distribution, but is still very poorly sorted. Sand contributes 76.6% to the total grain size distribution. The silt fraction is 22.8% of the total grain size distribution, and the clay fraction is 0.6%.

The ED-XRF results of the most abundant elements are displayed as percentages in Table 2. Outcrop and outer dune samples are rich in silicon dioxide (SiO_2). Aluminium oxide (Al_2O_3) is the second most abundant element in both the outcrop and outer dune samples. Inner dune samples from MLD 1 are composed mostly of SiO_2, followed by magnesium oxide (MgO) and calcium oxide (CaO). The MLD 1 samples also contain iron oxide (Fe_2O_3) and aluminium oxide (Al_2O_3). At MAR-T1, the CaO content increases with depth (Table 2).

SiO_2 is abundant at MAL Quarry, followed by CaO, MgO, and Al_2O_3, respectively (Table 2). However, the CaO content fluctuates throughout the profile. The MAL Quarry Bed 1 surface is composed of mostly SiO_2 followed by CaO. MAL Quarry Bed 3 has the lowest CaO percentage of the sequence, but it has a high SiO_2 content. The highest concentration of CaO in the MAL Quarry is in the lowermost layer of the sequence (Bed 5). MAL Quarry Bed 5, LET 1 Bed 2, and LET 1 Bed 3 are all pan samples that are cemented mostly by CaO (Table 2). MAL Quarry Bed 5 contains the greatest abundance of CaO and MgO out of all the samples (Table 2). The beds with the highest CaO content in LET are LET 1 Beds 2 and 3 and LET Profile 2. In LET Profile 1 Bed 1 and LET Profile 2, the

SiO_2 content is higher than the CaO content (Table 2). At both MAR-QCE1 and MAR-G1, the SiO_2 content is greater than the CaO content. MAR-G1 has high concentrations of MgO (Table 2).

Table 2. ED-XRF elemental analysis of major elements present throughout all the bulk sediment samples, from July/August 2022, with the results presented in percentages. The context and duricrust classification is also presented.

Site/sample	MgO	Al_2O_3	SiO_2	K_2O	CaO	Fe_2O_3	Classification
ITI-T1	0.1%	1.2%	79.4%	0.1%	0.1%	0.3%	Outcrop (unconsolidated sand)
MAL Quarry Bed 1 (surface)	2.7%	0.4%	36.3%	0.1%	10.2%	0.2%	Near surface calcrete or intergrade duricrust
MAL Quarry Bed 2	2.4%	0.4%	55.2%	0.1%	8.7%	0.2%	Intergrade duricrust
MAL Quarry Bed 3	3.5%	1.1%	82%	0.2%	1.8%	0.4%	Intergrade duricrust (compositionally more similar to silcrete with high SiO_2)
MAL Quarry Bed 4 (upper)	1.4%	0.4%	35.4%	0.1%	1.9%	0.2%	Intergrade duricrust
MAL Quarry Bed 4 (middle)	3.7%	0.7%	51.1%	0.1%	2.4%	0.3%	Intergrade duricrust
MAL Quarry Bed 4 (lower)	5.2%	1.0%	64.7%	0.2%	2.4%	0.3%	Intergrade duricrust
MAL Quarry Bed 5	15.1%	1.3%	19.2%	0.4%	22.4%	0.6%	Calcrete
MLD 1.1	1.7%	0.7%	56.0%	0.1%	0.9%	0.2%	Inner dune
MLD 1.2	1.7%	0.8%	83.7%	0.1%	1.5%	0.2%	Inner dune
MLD 1.3	2.4%	1.1%	89.5%	0.1%	1.9%	0.2%	Inner dune
MLD 1.4	2.4%	0.9%	76.2%	0.1%	1.7%	0.2%	Inner dune
LET Quarry Profile 1 Bed 1	5.6%	0.5%	33.9%	0.2%	9.3%	0.3	Intergrade duricrust or near surface calcrete
LET Quarry Profile 1 Bed 2	4.8%	0.8%	30.2%	0.3%	20.1%	0.4	Near-surface calcrete
LET Quarry Profile 1 Bed 3	7.9%	0.8%	19.2%	0.3%	14%	0.4%	Near-surface calcrete
LET Quarry Profile 2	3.3%	3.1%	58.9%	0.9%	18.7%	0.8%	Intergrade duricrust
MLD 2.1	0.4%	1.4%	78%	0.1%	0%	0.3%	Outer dune (sand)
MLD 2.2	0.5%	1.2%	60.6%	0.1%	0%	0.2%	Outer dune (sand)
MLD 2.3	0.6%	1.1%	68%	0.1%	0.1%	0.3%	Outer dune (sand)
MAR-QCE 1 surface	3.0%	1.0%	40.8%	0.8%	6.9%	0.8%	Intergrade duricrust
MAR-QCE 1 Bed 1	3.5%	3.4%	63.8%	1.5%	16%	1.2%	Intergrade duricrust
MAR-QCE 1 Bed 2	5.4%	5.0%	57.3%	2.2%	10.8%	2.1%	Intergrade duricrust
MAR-T1 Bed 1 upper	4.3%	1.4%	82.7%	0.4%	4.1%	0.5%	Inner dune
MAR-T1 Bed 1 lower	4.8%	1.3%	88.2%	0.3%	4.9%	0.5%	Inner dune
MAR-T1 Bed 2 (calcrete)	4.9%	1.1%	62.8%	0.5%	10.5%	0.5%	Inner dune
MAR-T2	0.1%	1.6%	64.7%	0.1%	0%	0.5%	Outcrop (unconsolidated sand)
MAR-G1 Bed 1	11.9%	2.0%	55.7%	0.6%	24%	0.8%	Intergrade duricrust or near surface calcrete
MAR-G1 Bed 2 (upper)	8.8%	1.9%	30.6%	0.6%	9.8%	1.1%	Calcite cemented sand
MAR-G1 Bed 2 (lower)	8.0%	2.3%	33.0%	0.7%	6.4%	1.9%	Calcite cemented sand
MAR-G1 Bed 3	4.2%	0.9%	28.6%	0.3%	4.7%	0.6%	Calcite cemented sand

Inner dune sediments differ from outer dune and outcrop sediments as they often contain elements present in the duricrusts (e.g., CaO). Outer dune and outcrop samples consist mainly of SiO_2 and do not overlap with the duricrust samples to the extent that the inner dune samples do (Table 2). Field observations (SOM 1 Table 1) and XRD results (SOM 1 Figs 2-10) were also taken into consideration when classifying duricrusts.

The PCA plot (Fig. 15) is based on quantitative data from XRF, LOI, and particle size analysis. Data were normalised in MS Excel using the logarithmic function. Principal component (PC) 1 and PC2 represent 68% of the total variance of the PCA plot. The PCA indicates that the samples form two distinct groups, separating duricrust samples from dune and outcrop samples. However, the inner dune samples from MAR-T1 have been grouped along with duricrust samples in the upper right quadrant. The PCA clusters the inner dune samples from MLD 1 closer to the duricrust samples (such as MAL Quarry Bed 3) rather than with the other dune samples. This suggests some overlap in chemical composition, but differences in particle sizes.

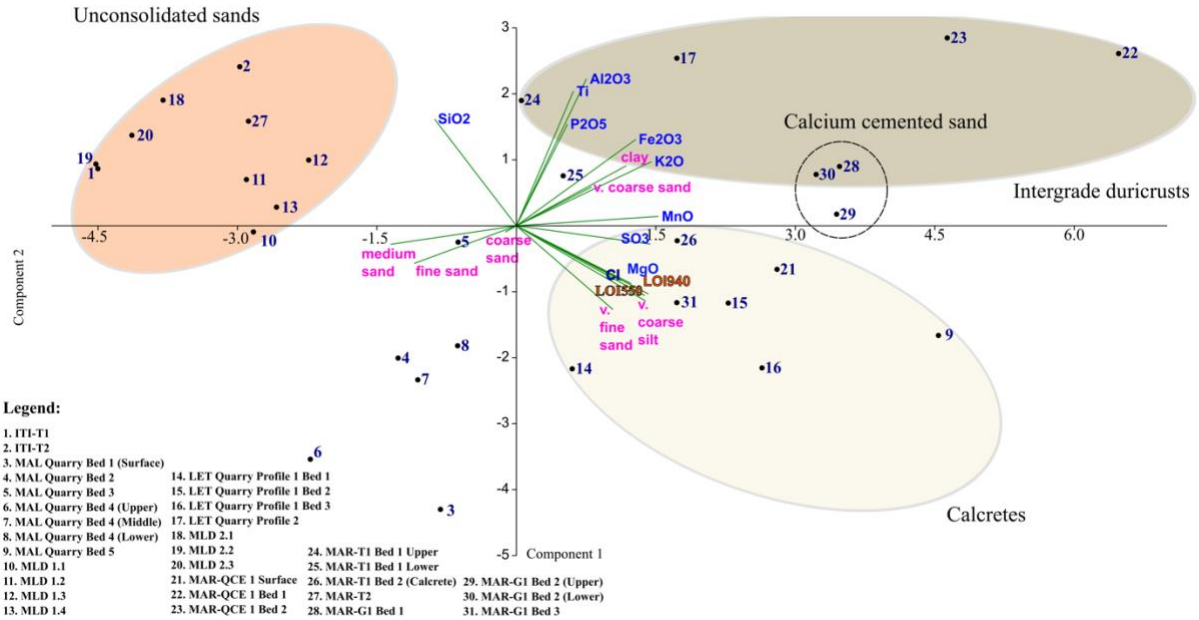

Figure 15. Principal Component Analysis plot based on XRF, LOI, and particle size data.

In the pan (duricrust) samples, calcite and quartz are omnipresent. MAR-G1 contains additional clay minerals, such as sepiolite, which is present in MAR-G1 Bed 2 (lower and upper) and Bed 3. Illite is only present in MAR-G1 Bed 2 (lower). Both calcite and quartz were identified in MAR-QCE 1. Quartz was identified in the dune (and outcrop) samples from MAR, however a difference is noted between inner sand accumulation samples (MAR-T1) and the other red sand (MAR-T2) samples. The clay mineral sepiolite (identified in the pans) is also present in MAR-T1 (Bed 1 lower, and Bed 2 [Calcrete]). The entire MAR-T1 sequence contains calcite. XRD graphs are provided in SOM 1 Figures 2-10.

Only the MAR samples from the pan contained microfossils, most notably the entire MAR-G1 sequence. The genus and species classification of the ostracods is uncertain, due to the ostracods still being in juvenile moulting stages and the valves being badly preserved, thus making taxonomic feature identification (such as ornamentation) difficult. The valves were mostly broken up into smaller, unidentifiable pieces, so taxonomic classifications had to be made using only those few valves with distinguishing morphological features. Despite these uncertainties, the ostracods do bear some morphological similarities to either cf. *Zonocypris* or cf. *Sarscypridopsis* (Fig. 16a). However, this preliminary classification should be approached with caution and adult specimens are necessary to make a definitive taxonomic analysis.

Diatoms were observed in the 63 µm and 125 µm fractions. Note that the samples were cleaned according to an ostracod cleaning protocol and more diatoms could therefore be expected in the sediment if a diatom processing protocol was applied. The diatoms belong to the taxon *Campylodiscus* sp. (Fig. 16b).

6. Discussion

The unconsolidated red sand samples (ITI-T1, MLD 2 & MAR-T2) can be categorised as Kalahari Sands subjected to aeolian processes (e.g., Mokatse et al. 2022). Kalahari sands often exhibit aeolian characteristics, frequently described as fine to medium sands with rounded to sub-rounded grains (Thomas & Shaw 1991; Haddon 2005). These sands may include a weathering component from underlying Karoo sandstones, as suggested by Thomas & Shaw (1991). This weathering component likely contributes to the occurrence of coarser particles in MAR-T2. The classification of ITI-T1, MLD 2 and MAR-T2 as Kalahari Sand is attributed to the relatively well-sorted, unimodal sediment distributions and the predominance of SiO_2 (quartz was also identified by the XRD analysis for MAR-

T2) (akin to descriptions by Thomas & Shaw 1991; Haddon 2005; Haddon & McCarthy 2005). A smaller silt fraction within the Kalahari sand samples can be associated with the input of aeolian dust (Thomas & Wiggs 2022). Lithic surface scatters on the outcrops (ITI-T1 & MAR-T2) are exposed due to aeolian erosion (deflation), causing heavier pieces to remain on the surface while lighter particles are transported away. Stone tools found below the surface in the test pits are not *in situ*, as the covering sediment is a Holocene occurrence. This will, however, require further testing alongside a high-resolution lithic analysis.

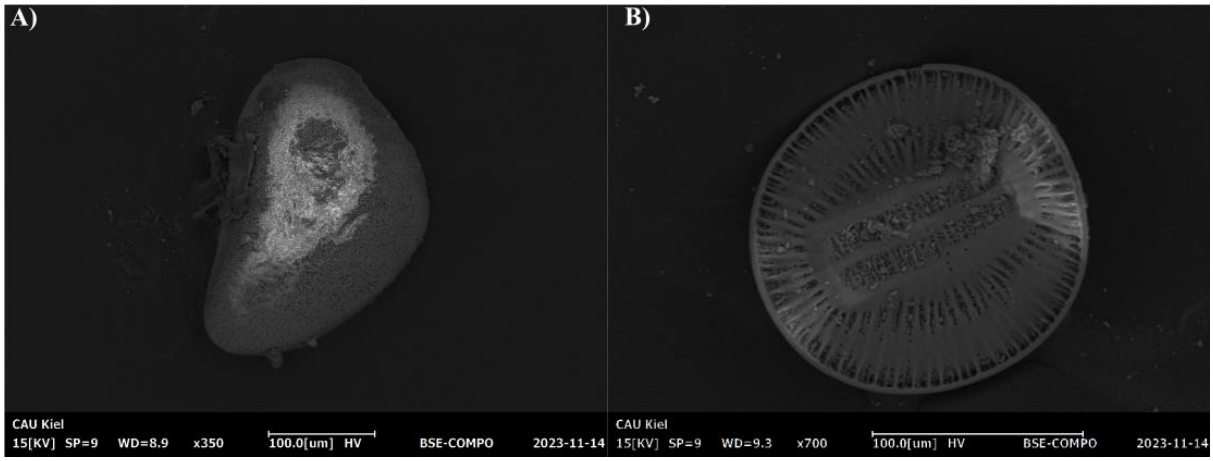

Figure 16. Microfossil taxa from MAR-G1. a) Ostracod from MAR-G1 Bed 2; b) *Campylodiscus* sp. from MAR-G1 Bed 2.

MLD 2 only contains trace amounts of CaO and the sediment is not the same pale colour as observed in the inner dunes and pans. A direct relationship between the outer dunes and pan sediment could not be established. Lancaster (1978) suggests that the red dunes result from Kalahari sand being deflated from the pan site and becoming enriched in red pigment as they age (Norris 1969). This is due to the weathering of iron oxides (Norris 1969; Haddon 2005) and climatic factors, such as periods of increased moisture availability and periodically warmer climates, which cause the dunes to become redder over time (Norris 1969). The sediment from the outer red dune (MLD 2) differs from the inner dunes, which have been deflated from the pans.

The inner dunes (MLD 1; MAR-T1) are poorly sorted, lighter in colour than the outer dunes, and contain CaO and clay minerals (sepiolite and calcite in the case of MAR-T1) likely deflated from the duricrusts in the pans, which is comparable to what Lancaster (1978) has described. The particle sizes of most samples from both MLD 1 and MAR-T1 are unimodal but poorly sorted, with most of the particles in the sand-size category. The lowermost bed of MAR-T1 (Bed 2) is an exception, as it has a bimodal distribution. MAR-T1 Bed 2 contains duricrust nodules, indicating that duricrust formation is a contributing factor to the bimodal particle size distribution and that there is pan sediment underneath the inner dune. The inner dune sediment from both Maleshe Pan (MLD 1) and Maralaleng Pan (MAR-T1) reflects a contribution of deflation and runoff processes during the wet season, as indicated by the poorly sorted sediment. Furthermore, Maralaleng Pan lacks clear dune accumulations, as the outcrop on the southwestern side of the site likely truncated the accumulation of the two ‘typical’ lunette dunes.

The CaO content varies between MLD 1 and MAR-T1. MAR-T1 is more enriched in CaO than MLD 1 samples and contains duricrust nodules in the lowermost bed. Like the outer dunes, the inner dunes are also Holocene accumulations, likely due to short phases of sediment wind transport and sediment runoff from water movement (see Schüller et al. 2022; Thomas & Wiggs 2022). The PCA groups dune and outcrop samples together, except MAR-T1, which is grouped along with duricrust samples, potentially suggesting new duricrust formation. Inner dune samples from MLD 1 are clustered closer to the duricrust sample MAL Quarry Bed 3 rather than the unconsolidated sand samples. The PCA

therefore confirms that there are similarities between the inner dunes and the duricrusts. Three distinct clusters are observed in the PCA, namely sandy samples, intergrade duricrusts, and calcretes (Fig. 15). However, despite being grouped with calcretes in the PCA, MAR-G1 Bed 3 has been classified as a calcium cemented sand, as denoted in field observations. However, field observations noted the increased presence of calcite nodules compared to the other samples. Duricrust samples, although more variable than dune samples, tend to be finer-grained (coarse silt and very coarse silt make up a portion of PC2). Inside the pans, sediment sorting is increasingly poor.

Most of the pan duricrusts discussed here are intergrade duricrusts, but where the sediment is more enriched in SiO_2 than CaO. Only a few samples (namely MAL Quarry Bed 5, LET Profile 1 Bed 2 & Bed 3) are calcretes, following the definition described in Watts (1980). Some duricrusts, such as MAL Quarry Bed 1 (surface) and LET Profile 1 Bed 1 may also be calcretes, as they are near the surface and contain CaO as a cementing agent. Without a micromorphological analysis, it is difficult to determine the exact duricrust category, as the silicification of calcretes or the calcification of silcretes is possible and is primarily identified in thin section (Nash & Shaw 1998). Due to the identification of calcite in MAR-G1, MAR-T1, and MAR-QCE 1, by XRD analysis, an inference that the CaO is related to $CaCO_3$ can be made.

The middle beds of MAL Quarry (MAL Quarry Bed 2, Bed 3, & Bed 4 [Upper]), the lower LET Quarry bed (LET Quarry Profile 1 Bed 3) and the MAR-G1 sequence could all be indicative of runoff processes. At MAR-G1 the particle size distributions in the upper samples are polymodal, suggesting multiple sediment inputs, while lower samples are unimodal. In the upper layers, water runoff during the rainy season can cause all particle sizes to be deposited (Schüller et al. 2022). The ostracod specimens in MAR-G1 Bed 1 are poorly preserved and the population structure, mostly juveniles and broken valves, reflects a taphocoenosis (Boomer et al. 2003) with post-depositional movement or diagenesis. A census count of ostracods was therefore not conducted for this contribution. The diatom taxon, *Campylodiscus* sp., has been noted in salt pans in South Africa (Taylor et al. 2007) and across Botswana (Ringrose et al. 2014; Szwarc et al. 2021; Szwarc & Namiotko 2022) indicating a brackish to saline environment (Gasse 2002; Nash & McLaren 2003). A very conservative taxonomic inference would be that the ostracod taxon is either from the genus *Zonocypri*, which indicates fresh to brackish water conditions (Martens et al. 1996, Szwarc & Namiotko 2022) or, that the specimens could belong to the genus *Sarscypridopsis*, which occurs in saline environments, and has been identified at Makgadikgadi (Franchi et al. 2022). Ostracods are often present in lacustrine environments and prefer a pH that is more alkaline rather than acidic. Ostracod valves usually dissolve in highly acidic environments (Griffiths & Holmes 2000). MAR-G1 is more similar to a calcrete than a silcrete, and the presence of the ostracod valves suggest a pH that was not too acidic for ostracods to live in and was also sufficient for valve preservation. The presence of the microfossils and particle sizes in the lower beds of MAR-G1 suggest that this waterbody existed for a long enough period to sustain microfossil populations.

The pan sediments from our region, albeit unimodal in some cases, are generally poorly sorted. Burrough et al. (2009) report that grains at Makgadikgadi became larger and more poorly sorted when cal-silcrete was present, due to the presence of shell, nodules and roots. This could be a possible explanation for larger particle sizes reported in the pans where the intergrade duricrusts are observed. Sepiolite, found in MAR-G1 and MAR-T1, can form in more alkaline conditions than palygorskite under direct precipitation (Watts 1980). Sepiolite and $CaCO_3$ (and by inference, calcite) both precipitate during the dry season (Wang et al. 1994). The presence of sepiolite in both MAR-T1 and MAR-G1 suggest that pan sediment likely deflated from the vicinity of MAR-G1 and was redeposited in MAR-T1. Sepiolite is an authigenic clay mineral often associated with lacustrine environments (such as pans) in semi-arid regions and has been noted in mature calcrete profiles (Watts 1980). The present results suggest various site formation processes across the study region, of which run-off, deflation, and varying pH levels are prominent. These proxies assist in inferring a brackish to saline lacustrine environment when MSA hominins occupied and exploited the landscape.

7. Conclusions

Three main site formation processes have been identified at archaeological sites in the Kgalagadi district, namely runoff, deflation, and duricrust formation. Outcrops and dunes have undergone aeolian deposition or reworking, likely due to sediment deflation. An example that fits descriptions in the literature of this deflation process can be observed at MLD 1 and MAR-T1. Despite the lack of a clear set of lunette dunes at MAR, the role of deflation and aeolian input can still be observed from the particle size data. The outcrop to the south-west of Maralaleng likely stopped sediment from accumulating into a lunette dune, like those found at Maleshe Pan.

These results show that the sediment at each dune and outcrop site is moderately well sorted with unimodal distributions. However, the sediment becomes more poorly sorted, and the occurrence of polymodal distributions increases towards the pans where duricrusts are present. At Maleshe Pan and Maralaleng Pan, surface runoff during the rainy season moves moderately well-sorted sediment from the dunes and outcrops towards the pans, depositing various grain sizes and causing polymodal distributions. The formation of the pans is associated with their locations at low-lying sections of basins, but the role of the water table and other hydrological factors will be analysed in a future micromorphological study.

This research investigated the mechanisms involved in the deposition of the pan, dune, and outcrop sediment, and highlights depositional mechanisms: the deflation of sediment from pans onto the inner dunes, the deflation of sediment on the outcrops leading to the exposure of lithics on the surface, and runoff causing sediment to be taken from the dunes back into the pans, leading to polymodal and/or poorly sorted sediment. The pans were the first to form (suggesting that the occurrence of the lithics in the vicinity is due to the presence of hominins around a body of water) followed by the dunes.

Acknowledgements

This research was conducted under the research permit ENT 8/36/4 L (56), issued on 26 August 2021 by the Botswana Ministry of Environment, Wildlife and Tourism. The project is funded by the Deutsche Forschungsgemeinschaft (DFG, German Research Foundation) under grant number 455851250. The Department of Monuments at the National Museum of Botswana, the University of Botswana, and the McGregor Museum in Kimberley are all appreciated for providing laboratory space, vehicles, equipment, and storage. We value the diligence and hard work put forth by Thuto Isaac Kgannyeng and Boipuso Fox. Our appreciation goes to Keneilwe Petlo, Masa Kedisang, Idah Maniki, Tsephang Dinake, Mariaan de Bruin, Helena Pribliczki and Rowena Winterhalder for their contributions to our 2022 field season. The contributions of the Maleshe, Maralaleng, Maubelo and Tsabong communities were integral to the success of our research and are greatly appreciated. The authors also express their gratitude to Yasmin Dannath for her assistance with the SEM. The authors appreciate the work of Brendan Ledwig, University Kiel, Institute of Geosciences, Mineralogy working group, for his assistance with the processing of the XRD samples and determining mineral presence. The assistance and patience of Prof. David Nash with duricrust related questions is also appreciated. And lastly, the authors would like to thank the reviewers and journal editors for their time and contributions to the article.

Supporting online material

Faul et al. Supporting Online Material File 1
Faul et al. Supporting Online Material File 2

References

Alonso-Zarza, A.M. & Wright, V.P. 2010. Calcretes. Developments in Sedimentology, 61: 225-267. https://doi.org/10.1016/S0070-4571(09)06105-6

Berna, F., Goldberg, P., Horwitz, L.K., et al. 2012. Microstratigraphic evidence of *in situ* fire in the Acheulean strata of Wonderwerk Cave, Northern Cape province, South Africa. Proceedings of the National Academy of Sciences, 109(20): E1215-E1220. https://doi.org/10.1073/pnas.1117620109

Bialik, O.M., Jarochowska, E. & Grossowicz, M. 2021. Ordination analysis in sedimentology, geochemistry and

palaeoenvironment – Background, current trends and recommendations. The Depositional Record, 7(3): 541-563. https://doi.org/10.1002/dep2.161

Blott, S.J. & Pye, K. 2001. GRADISTAT: A grain size distribution and statistics package for the analysis of unconsolidated sediments. Earth Surface Processes and Landforms, 26(11): 1237-1248. https://doi.org/10.1002/esp.261

Boomer, I., Horne, D.J. & Slipper, I.J. 2003. The use of ostracods in palaeoenvironmental studies, or what can you do with an ostracod shell? The Paleontological Society Papers, 9: 153-180. https://doi.org/10.1017/S1089332600002199

Bowler, J.M. 1986. Spatial variability and hydrologic evolution of Australian lake basins: Analogue for Pleistocene hydrologic change and evaporite formation. Palaeogeography, Palaeoclimatology, Palaeoecology, 54(1-4): 21-41. https://doi.org/10.1016/0031-0182(86)90116-1

Burrough, S.L., Thomas, D.S., Allin, J.R., et al. 2022. Lessons from a lakebed: Unpicking hydrological change and early human landscape use in the Makgadikgadi basin, Botswana. Quaternary Science Reviews, 291: 107662. https://doi.org/10.1016/j.quascirev.2022.107662

Burrough, S.L., Thomas, D.S. & Bailey, R.M. 2009. Mega-Lake in the Kalahari: A Late Pleistocene record of the Palaeolake Makgadikgadi system. Quaternary Science Reviews, 28(15-16): 1392-1411. https://doi.org/10.1016/j.quascirev.2009.02.007

Byakatonda, J., Parida, B.P., Kenabatho, P.K., et al. 2018. Influence of climate variability and length of rainy season on crop yields in semiarid Botswana. Agricultural and Forest Meteorology, 248: 130-144. https://doi.org/10.1016/j.agrformet.2017.09.016

Degen, T., Sadki, M., Bron, E., et al. 2014. The HighScore suite. Powder Diffraction, 29(S2): S13-S18. https://doi.org/10.1017/S0885715614000840

Ecker, M., Green, C., Henderson, A., et al. 2023. Archaeological survey near Tsabong, Kgalagadi District, southwestern Botswana. Azania: Archaeological Research in Africa, 58: 1-19. https://doi.org/10.1080/0067270X.2023.2260150

Filzmoser, P., Hron, K. & Reimann, C. 2009. Principal component analysis for compositional data with outliers. Environmetrics, 20: 621-632. https://doi.org/10.1002/env.966

Folk, R.L. & Ward, W.C. 1957. Brazos River bar: A study in the significance of grain size parameters. Journal of Sedimentary Petrology, 27: 3-26.

Franchi, F., Cavalazzi, B., Evans, M., et al. 2022. Late Pleistocene – Holocene palaeoenvironmental evolution of the Makgadikgadi Basin, Central Kalahari, Botswana: New evidence from shallow sediments and ostracod fauna. Frontiers in Ecology and Evolution, 10: 818417. https://doi.org/10.3389/fevo.2022.818417

Gasse, F. 2002. Diatom-inferred salinity and carbonate oxygen isotopes in Holocene waterbodies of the western Sahara and Sahel (Africa). Quaternary Science Reviews, 21: 737-767. https://doi.org/10.1016/S0277-3791(01)00125-1

Goudie, A. 1972. The chemistry of world calcrete deposits. The Journal of Geology, 80(4): 449-463. https://doi.org/10.1086/627766

Griffiths, H.I. & Holmes, J.A. 2000. Non-marine Ostracods and Quaternary Palaeoenvironments: Technical Guide 8. London: Quaternary Research Association.

Grün, R., Brink, J.S., Spooner, N.A., et al. 1996. Direct dating of Florisbad hominid. Nature, 382(6591): 500-501. https://doi.org/10.1038/382500a0

Haddon, I.G. 2005. The sub-Kalahari geology and tectonic evolution of the Kalahari Basin, southern Africa. Doctoral Thesis. Johannesburg: University of the Witwatersrand.

Haddon, I.G. & McCarthy, T.S. 2005. The Mesozoic – Cenozoic interior sag basins of Central Africa: The late-cretaceous – Cenozoic Kalahari and Okavango basins. Journal of African Earth Sciences, 43(1-3): 316-333. https://doi.org/10.1016/j.jafrearsci.2005.07.008

Hammer, Ø. & Harper, D.A. 2001. PAST: Paleontological Statistics Software Package for education and data analysis. Palaeontologia Electronica, 4(1): 1-9. https://palaeo-electronica.org/2001_1/past/past.pdf

Heiri, O., Lotter, A.F. & Lemcke, G. 2001. Loss on ignition as a method for estimating organic and carbonate content in sediments: Reproducibility and comparability of results. Journal of Paleolimnology, 25: 101-110. https://doi.org/10.1023/A:1008119611481

Helgren, D.M. & Brooks, A.S. 1983. Geoarchaeology at Gi, a Middle Stone Age and Later Stone Age site in the northwest Kalahari. Journal of Archaeological Science, 10: 181-197. https://doi.org/10.1016/0305-4403(83)90051-1

Henshilwood, C.S., d'Errico, F., Van Niekerk, K.L., et al. 2018. An abstract drawing from the 73,000-year-old levels at Blombos Cave, South Africa. Nature, 562(7725): 115-118. https://doi.org/10.1038/s41586-018-0514-3

Hills, E.S. 1940. The lunette, a new land form of aeolian origin. Australian Geographer, 3(7): 15-21.

https://doi.org/10.1080/00049184008702196
Horne, D.J. & Siveter, D.J. 2016. Collecting and processing fossil ostracods. Journal of Crustacean Biology, 36(6): 841-848. https://doi.org/10.1163/1937240X-00002487
Kampunzu, A.B., Ringrose, S., Huntsman-Mapila, P., et al. 2007. Origins and palaeo-environments of Kalahari duricrusts in the Moshaweng dry valleys (Botswana) as detected by major and trace element composition. Journal of African Earth Sciences, 48(2-3): 199-221. https://doi.org/10.1016/j.jafrearsci.2006.10.007
Kuman, K., Lotter, M.G. & Leader, G.M. 2020. The Fauresmith of South Africa: A new assemblage from Canteen Kopje and significance of the technology in human and cultural evolution. Journal of Human Evolution, 148: 102884. https://doi.org/10.1016/j.jhevol.2020.102884
Lancaster, I.N. 1978. The pans of the southern Kalahari, Botswana. Geographical Journal, 144: 81-98. https://doi.org/10.2307/634651
Lukich, V. 2019. Palaeoenvironmental reconstruction and geochronology of the archaeological localities at Kathu Pan, South Africa. Doctoral Thesis. Toronto: University of Toronto.
Lukich, V. & Ecker, M. 2022. Pleistocene environments in the southern Kalahari of South Africa. Quaternary International, 614: 50-58. https://doi.org/10.1016/j.quaint.2021.03.008
Lukich, V., Cowling, S. & Chazan, M. 2020. Palaeoenvironmental reconstruction of Kathu Pan, South Africa, based on sedimentological data. Quaternary Science Reviews, 230: 106153. https://doi.org/10.1016/j.quascirev.2019.106153
Marean, C.W. 2010. Pinnacle Point Cave 13B (Western Cape Province, South Africa) in context: The Cape floral kingdom, shellfish, and modern human origins. Journal of Human Evolution, 59(3-4): 425-443. https://doi.org/10.1016/j.jhevol.2010.07.011
Martens, K., Davies, B.R., Baxter, A.J., et al. 1996. A contribution to the taxonomy and ecology of the Ostracoda (Crustacea) from Verlorenvlei (Western Cape, South Africa). African Zoology, 31(1): 22-36. https://www.ajol.info/index.php/az/article/view/154384
Mokatse, T., Diaz, N., Shemang, E., et al. 2022. Landscapes and landforms of the Chobe enclave, northern Botswana. In: Eckardt, F.D. (ed.) Landscapes and Landforms of Botswana. World Geomorphological Landscapes: 91-116. Cham: Springer International Publishing. https://doi.org/10.1007/978-3-030-86102-5_6
Munyikwa, K., Van Den Haute, P., Vandenberghe, D., et al. 2000. The age and palaeoenvironmental significance of the Kalahari Sands in western Zimbabwe: A thermoluminescence reconnaissance study. Journal of African Earth Sciences, 30(4): 941-956. https://doi.org/10.1016/S0899-5362(00)00062-2
Nash, D.J. 2022. Calcretes, silcretes and intergrade duricrusts. In: Eckardt, F.D. (ed.) Landscapes and Landforms of Botswana. World Geomorphological Landscapes: 223-246. Cham: Springer International Publishing. https://doi.org/10.1007/978-3-030-86102-5_13
Nash, D.J., Ciborowski, T.J.R., Coulson, S.D., et al. 2022. Mapping Middle Stone Age human mobility in the Makgadikgadi Pans (Botswana) through multi-site geochemical provenancing of silcrete artefacts. Quaternary Science Reviews, 297: 107811. https://doi.org/10.1016/j.quascirev.2022.107811
Nash, D.J. & McLaren, S.J. 2003. Kalahari valley calcretes: Their nature, origins, and environmental significance. Quaternary International, 111(1): 3-22. https://doi.org/10.1016/S1040-6182(03)00011-9
Nash, D.J., McLaren, S.J. & Webb, J.A. 2004. Petrology, geochemistry and environmental significance of silcrete-calcrete intergrade duricrusts at Kang Pan and Tswaane, central Kalahari, Botswana. Earth Surface Processes and Landforms, 29(12):1559-1586. https://doi.org/10.1002/esp.1138
Nash, D.J. & Shaw, P.A. 1998. Silica and carbonate relationships in silcrete-calcrete intergrade duricrusts from the Kalahari of Botswana and Namibia. Journal of African Earth Sciences, 27(1): 11-25. https://doi.org/10.1016/S0899-5362(98)00043-8
Nash, D.J., Shaw, P.A. & Thomas, D.S. 1994. Duricrust development and valley evolution: Process – landform links in the kalahari. Earth Surface Processes and Landforms, 19(4): 299-317. https://doi.org/10.1002/esp.3290190403
Netterberg, F. 1969. Ages of calcretes in southern Africa. South African Archaeological Bulletin, 24: 88-92. https://doi.org/10.2307/3888283
Netterberg, F. 1980. Geology of southern African calcretes. 1: Terminology, description, macrofeatures, and classification. South African Journal of Geology, 83(2): 255-283. https://hdl.handle.net/10520/AJA10120750_1202
Norris, R.M. 1969. Dune reddening and time. Journal of Sedimentary Research, 39(1): 7-11.
Planchon, O. & Darboux, F. 2002. A fast, simple and versatile algorithm to fill the depressions of digital elevation models. Catena, 46(2): 159-176. https://doi.org/10.1016/S0341-8162(01)00164-3
Ringrose, S., Cassidy, L., Diskin, S., et al. 2014. Diagenetic transformations and silcrete-calcrete intergrade duricrust formation in palaeo-estuary sediments. Earth Surface Processes and Landforms, 39(9): 1167-

1187. https://doi.org/10.1002/esp.3516
Ringrose, S., Downey, B., Genecke, D., et al. 1999. Nature of sedimentary deposits in the western Makgadikgadi basin, Botswana. Journal of Arid Environments, 43(4): 375-397. https://doi.org/10.1006/jare.1999.0548
Rutherford, M.C., Mucina, L. & Powrie, L.W. 2006. Biomes and bioregions of southern Africa. In: Rutherford, M.C. & Mucina, L. (eds) The Vegetation of South Africa, Lesotho and Swaziland: 30-51. Pretoria: South African National Biodiversity Institute.
Schüller, I., Belz, L., Wilkes, H., et al. 2022. Kalahari pans: Quaternary evolution and processes of ephemeral lakes. In: Eckardt, F.D. (ed.) Landscapes and Landforms of Botswana. World Geomorphological Landscapes: 167-178. Cham: Springer International Publishing. https://doi.org/10.1007/978-3-030-86102-5_10
Shaw, P. & Thomas, D.S.G. 1997. Pans, playas and salt lakes. In: Goudie, A. (ed.) Arid Zone Geomorphology: Process, Form and Change in Drylands 2nd Edition: 293-317. John Wiley & Sons Ltd. https://doi.org/10.1002/9780470710777.ch15
Sievers, C., Backwell, L., d'Errico, F., et al. 2022. Plant bedding construction between 60,000 and 40,000 years ago at Border Cave, South Africa. Quaternary Science Reviews, 275: 107280. https://doi.org/10.1016/j.quascirev.2021.107280
Staurset, S., Coulson, S.D., Mothulatshipi, S., et al. 2023. Making points: The Middle Stone Age lithic industry of the Makgadikgadi Basin, Botswana. Quaternary Science Reviews, 301: 107823. https://doi.org/10.1016/j.quascirev.2022.107823
Summerfield, M.A. 1983a. Silcrete as a palaeoclimatic indicator: Evidence from southern Africa. Palaeogeography, Palaeoclimatology, Palaeoecology, 41(1-2): 65-79. https://doi.org/10.1016/0031-0182(83)90076-7
Summerfield, M.A. 1983b. Silcrete. In: Goudie, A.S. & Pye, K. (eds) Chemical Sediments and Geomorphology: 59-93. London: Academic Press.
Szwarc, A., Martens, K. & Namiotko, T. 2021. Two new Cypridopsinae Kaufmann, 1900 (Crustacea, Ostracoda) from southern Africa. ZooKeys, 1076: 83-107. https://doi.org/10.3897/zookeys.1076.76123
Szwarc, A. & Namiotko, T. 2022. Biodiversity of non-marine Ostracoda (Crustacea) of Botswana: An annotated checklist with notes on distribution. Water, 14(9): 1441. https://doi.org/10.3390/w14091441
Tarboton, D. G., Bras, R.L., & Rodriguez-Iturbe, I. 1991. On the extraction of channel networks from digital elevation data. Hydrological Processes, 5: 81-100. https://doi.org/10.1002/hyp.3360050107
Taylor, J.C., Harding, W.R. & Archibald, C.G.M. 2007. An Illustrated Guide to Some Common Diatom Species from South Africa. Pretoria: Water Research Commission.
Telfer, M.W. & Thomas, D.S.G. 2006. Complex Holocene lunette dune development, South Africa: Implications for paleoclimate and models of pan development in arid regions. Geology, 34(10): 853-856. https://doi.org/10.1130/G22791.1
Telfer, M.W., Thomas, D.S.G., Parker, A.G., Walkington, H. and Finch, A.A. 2009. Optically Stimulated Luminescence (OSL) dating and palaeoenvironmental studies of pan (playa) sediment from Witpan, South Africa. Palaeogeography, Palaeoclimatology, Palaeoecology, 273(1-2).50-60.https://doi.org/10.1016/j.palaeo.2008.11.012
Thomas, D.S. 1988. The nature and depositional setting of arid and semi-arid Kalahari sediments, southern Africa. Journal of Arid Environments, 14(1): 17-26. https://doi.org/10.1016/S0140-1963(18)31092-9
Thomas, D. & Shaw, P.A. 1991. The Kalahari Environment. Cambridge: Cambridge University Press.
Thomas, D.S. & Wiggs, G.F. 2022. Dunes of the Southern Kalahari. In: Eckardt, F.D. (ed.) Landscapes and Landforms of Botswana. World Geomorphological Landscapes: 131-154. Cham: Springer International Publishing. https://doi.org/10.1007/978-3-030-86102-5_8
Thomas, D.S., Burrough, S.L., Coulson, S.D., et al. 2022. Lacustrine geoarchaeology in the central Kalahari: Implications for Middle Stone Age behaviour and adaptation in dryland conditions. Quaternary Science Reviews, 297: 107826. https://doi.org/10.1016/j.quascirev.2022.107826
Tidi, K.J. 1994. A Report on Geological Investigation in the Tsabong Area. Gaborone: Department of Geological Survey.
Toffolo, M.B., Brink, J.S., van Huyssteen, C., et al. 2017. A microstratigraphic reevaluation of the Florisbad spring site, Free State Province, South Africa: Formation processes and paleoenvironment. Geoarchaeology, 32(4): 456-478. https://doi.org/10.1002/gea.21616
Udden, J.A. 1914. Mechanical composition of clastic sediments. Bulletin of the Geological Society of America, 25(1): 655-744. https://doi.org/10.1130/GSAB-25-655
Wang, Y., Nahon, D. & Merino, E. 1994. Dynamic model of the genesis of calcretes replacing silicate rocks in semi-arid regions. Geochimica et Cosmochimica Acta, 58(23): 5131-5145. https://doi.org/10.1016/0016-7037(94)90299-2

Warren, J.K. 1983. Pedogenic calcrete as it occurs in Quaternary calcareous dunes in coastal South Australia. Journal of Sedimentary Research, 53(3): 787-796. https://doi.org/10.1306/212F82BF-2B24-11D7-8648000102C1865D

Watts, N.L. 1980. Quaternary pedogenic calcretes from the Kalahari (southern Africa): Mineralogy, genesis and diagenesis. Sedimentology, 27(6): 661-686. https://doi.org/10.1111/j.1365-3091.1980.tb01654.x

Webb, J.A. & Nash, D.J. 2020. Reassessing southern African silcrete geochemistry: Implications for silcrete origin and sourcing of silcrete artefacts. Earth Surface Processes and Landforms, 45(13): 3396-3413. https://doi.org/10.1002/esp.4976

Wentworth, C.K. 1922. A scale of grade and class terms for clastic sediments. Journal of Geology, 30: 377-392. https://doi.org/10.1086/622910

Werger, M.J.A. 1978. Vegetation structure in the southern Kalahari. The Journal of Ecology, 66(3): 933-941. https://doi.org/10.2307/2259305

Wilkins, J. 2017. Middle Pleistocene lithic raw material foraging strategies at Kathu Pan 1, Northern Cape, South Africa. Journal of Archaeological Science: Reports, 11: 169-188. https://doi.org/10.1016/j.jasrep.2016.11.002

Wilkins, J. 2023. Ga-Mohana Hill North Rockshelter, South Africa. In: Beyin, A., Wright, D.K., Wilkins, J., et al. (eds) Handbook of Pleistocene Archaeology of Africa: Hominin Behavior, Geography, and Chronology: 1469-1480. Cham: Springer International Publishing. https://doi.org/10.1007/978-3-031-20290-2_94

Wilkins, J., Schoville, B.J., Pickering, R., et al. 2021. Innovative *Homo sapiens* behaviours 105,000 years ago in a wetter Kalahari. Nature, 592(7853): 248-252. https://doi.org/10.1038/s41586-021-03419-0

Winterhalder, R. 2023. Treasure between rubble: Lithics from Itireleng and Maralaleng, southern Kalahari, Botswana. Masters Dissertation. Kiel: Kiel University.

Wurz, S. 2008. Modern behaviour at Klasies river. Goodwin Series, 10: 150-156. https://www.jstor.org/stable/40650026